University of Zurich[UZH]

Suppression of excited Onia States at the LHCb Experiment

Bachelor Thesis

of

Moritz Küng

Mathematisch-naturwissenschaftliche Fakultät

der

Universität Zürich

Prof. Dr. U. Straumann

Dr. O. Steinkamp

Ch. Elsasser

Zürich

2012

A measurement of the suppression factor between the different $\Upsilon(nS)$- and $\psi(nS)$-resonances in proton-proton collisions at a center-of-mass energy of 7 TeV is performed with data collected with the LHCb detector at the LHC. The quarkonia are reconstructed in the $\mu^+\mu^-$ decay channel, have momenta in the range from 2 GeV/c to 500 GeV/c and a pseudo rapidity between 2 and 4.5. The ratio of the $\Upsilon(2S)$ and $\Upsilon(3S)$ excited states to the $\Upsilon(1S)$ ground state is found to be $\Upsilon(2S+3S)/\Upsilon(1S) = 0.489 \pm 0.004_{\text{stat}} \pm 0.021_{\text{sys}} \pm 0.034_{\mathcal{B}}$ with the systematical uncertainty, which is the combination of trigger, selection and reconstruction efficiencies uncertainties and the uncertainty on the branching fractions to $\mu^+\mu^-$.
The ratio of the $\psi(2S)$ to the $J/\psi(1S)$ is found to be $\psi(2S)/J/\psi(1S) = 0.184 \pm 0.013_{\text{stat}} \pm 0.024_{\text{sys}} \pm 0.019_{\mathcal{B}} \pm 0.017_{\text{prompt}}$ with the additional uncertainty due to the correction for non-prompt charmonia.

Acknowledgement

First of all I would like to thank several people, who enabled this thesis and who supported me during the time I worked on this paper. I thank Prof. Dr. Ulrich Straumann and Dr. Olaf Steinkamp, who made it possible to write my bachelor thesis in the LHCb Group. A special thank goes to my advisor Christian Elsasser. His excellent support and the offer of his expertise have always been a great help when I had problems questions.
Further I would like to mention the people of our office, who helped me with computer issues and always made time for me: Roman Gredig, Arno Gadola, Nicola Chiapolini, Marco Tresch, Ben Huber and Christian Elsasser. It has been a great time and I thank you for the support and the great atmosphere.

Contents

Introduction

This thesis studies the suppression of excited vector bottomium and charmonium states with respect to the corresponding ground states. It is organized in the following manner: In the first chapter, the theory will be explained and I will give a short motivation, why we do this analysis. In the following chapter, I illustrate the LHCb detector.
Chapter 3 and Chapter 4 describe the analysis of the quarkonium suppression, including corrections for the trigger, selection and reconstruction efficiency as well as for the final state radiation in case of charmonium. The conclusion is a short summary of the results.

1 Theory

1.1 Standard Model

The Standard Model of particle physics describes the elementary particles and their interactions. It contains three generations of fermions and the gauge bosons. There exists to each fermion an antiparticle having the same qualities, but opposite charge-like quantum numbers. Table 1.1 lists all known fermions f (the antifermions $\overline{f}$ are not listed):

Quantity	1st generation	2nd generation	3rd generation
		Quarks	
	up (u)	charm (c)	top (t)
Q	$+2/3$	$+2/3$	$+2/3$
m	$2.3\,\mathrm{MeV/c^2}$	$1.275\,\mathrm{GeV/c^2}$	$173.5\,\mathrm{GeV/c^2}$
	down (d)	strange (s)	bottom or beauty (b)
Q	$-1/3$	$-1/3$	$-1/3$
m	$4.8\,\mathrm{MeV/c^2}$	$95\,\mathrm{MeV/c^2}$	$4.18\,\mathrm{GeV/c^2}$
		Leptons	
	electron (e^-)	muon (μ^-)	tau (τ^-)
Q	-1	-1	-1
m	$511\,\mathrm{keV/c^2}$	$106\,\mathrm{MeV/c^2}$	$1.78\,\mathrm{GeV/c^2}$
	electron-neutrino (ν_e)	muon-neutrino (ν_μ)	tau-neutrino (ν_τ)
Q	0	0	0
m	$< 2\,\mathrm{eV/c^2}$ 95% C.L.	$< 0.19\,\mathrm{MeV/c^2}$ 90% C.L.	$< 18.2\,\mathrm{MeV/c^2}$ 95% C.L.

Table 1.1: Fermions of the Standard Model [5].

1.2 Quarkonia or $c\bar{c}$- and $b\bar{b}$-Mesons

Like positronium which is a bound state of an electron and its antiparticle, the positron, quark-antiquark pairs can form an atomlike meson, called quarkonium. It consists for example of a b- and a $\bar{b}$-quark (Bottomonium). Table 1.2 shows a list of the quarkonia we are interested in for this paper: The two vector charmonia $J/\psi(1S)$ and $\psi(2S)$ as well as the three vector bottomonia $\Upsilon(1S)$, $\Upsilon(2S)$ and $\Upsilon(3S)$. They all have as vector mesons total spin $J = 1$, $J/\psi(1S)$ and $\psi(2S)$ as well as $\Upsilon(1S)$, $\Upsilon(2S)$ and $\Upsilon(3S)$ only differ in the radial excitation indicated by the integer number in their naming, which is the reason for their different masses. The $c\bar{c}$- and $b\bar{b}$-mesons mainly decay through the strong and electromagnetic interaction, hence the small lifetime.

Particle	QC	Mass m	Lifetime τ [1]	$\mathcal{B}(X \to \mu^+\mu^-)$
$c\bar{c}$-Mesons (Charmonia)				
$J/\psi(1S)$	$\lvert c\bar{c}\rangle$	$3096.9\,\mathrm{MeV/c^2}$	$7.1 \times 10^{-21}\,\mathrm{s}$	5.93 ± 0.06 %
$\psi(2S)$	$\lvert c\bar{c}\rangle$	$3686.1\,\mathrm{MeV/c^2}$	$2.2 \times 10^{-21}\,\mathrm{s}$	0.77 ± 0.08 %
$b\bar{b}$-Mesons (Bottomonia)				
$\Upsilon(1S)$	$\lvert b\bar{b}\rangle$	$9460.3\,\mathrm{MeV/c^2}$	$1.2 \times 10^{-20}\,\mathrm{s}$	2.48 ± 0.05 %
$\Upsilon(2S)$	$\lvert b\bar{b}\rangle$	$10\,023.3\,\mathrm{MeV/c^2}$	$2.1 \times 10^{-20}\,\mathrm{s}$	1.93 ± 0.17 %
$\Upsilon(3S)$	$\lvert b\bar{b}\rangle$	$10\,355.2\,\mathrm{MeV/c^2}$	$3.2 \times 10^{-20}\,\mathrm{s}$	2.18 ± 0.21 %

Table 1.2: List of vectorlike Charmonia and Bottomonia , $\mathcal{B}$ is the branching fraction, QC the quark configuration [5].

In the proton-proton collisions, the quarkonia mainly are produced through an annihilation of a valence quark with a sea quark of the same flavour, see Fig. 1.1. We analyse the decay chanels $\Upsilon(nS) \to \mu^+\mu^-$ and $\psi(nS) \to \mu^+\mu^-$ with the branching fractions shown in Table 1.2.

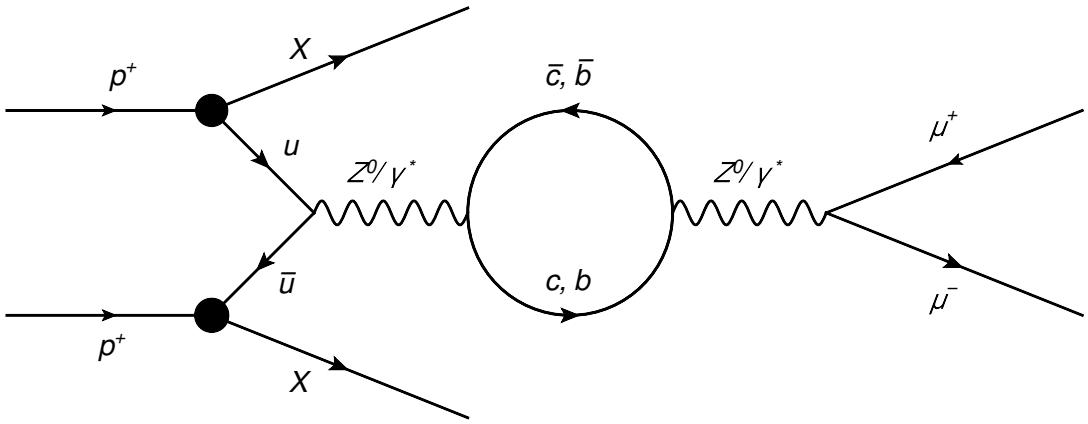

Figure 1.1: Feynman diagram of the production and decay of charmonium and bottomonium

1.3 Onia States and Quark-Gluon Plasma

In heavy ion collisions (for example Pb-Pb collisions at LHC) at high relativistic energies, the so-called quark-gluon plasma (QGP) is expected to be generated. The QGP is a speacial phase in quantum chromodynamics, which only exists at very high temperature or density. In this deconfined state, quarks and gluons are no longer bound in hadrons, but they are free. The phase transition between bound and unbound partons should occur at a critical temperature $T_C \simeq 170\,\mathrm{MeV}$ [2]. Different quarkonium states should therefore melt at different termperatures in the QGP because of the different strenght of the binding between quark and anti-quark. The $\Upsilon(1S)$ is strongly bound and should melt at $4.10T_C$, the $\Upsilon(2S)$ at $1.6T_C$ and the $\Upsilon(3S)$ at $1.2T_C$ [13]. This would lead to a suppression of quarkonium states in heavy ion collisions (and the generated QGP) and consequently we would observe an enhanced suppression of the $2S + 3S$ relative to the $1S$ ground state of the Υ-meson because of the lower melting points. If we calculate the radial wave functions of the $\Upsilon(1S)$, $\Upsilon(2S)$ and $\Upsilon(3S)$ for $T = 0\,\mathrm{MeV}$ and

[1] $\tau = \hbar/\Gamma$

[2] We use the convention $k_B = 1$.

$T = 200\,\text{MeV}$ we can see a different behaviour. The rms radius $\langle r^2\rangle^{1/2}$ of the ground state remains nearly unchanged, whereas the rms radii of $\Upsilon(2S)$ and, in particular, $\Upsilon(3S)$ state strongly depend on the temperature T of the QGP:

Temperature [MeV]	rms radii $\langle r^2\rangle^{1/2}$		
	$\Upsilon(1S)$	$\Upsilon(2S)$	$\Upsilon(3S)$
0	0.22	0.50	0.73
200	0.25	0.77	1.99

Table 1.3: The rms radii $\langle r^2\rangle^{1/2}$ of the radial wave functions of the $\Upsilon(1S)$, $\Upsilon(2S)$ and $\Upsilon(3S)$ states [6].

This is a hint, why the ratio $\Upsilon(2S+3S)/\Upsilon(1S)$ changes with the temperature T. Theoretical calculations have given the predictions listed in Table 1.4 for the bottomonium suppression in Pb-Pb collisions.

T_0 [MeV]	$\Upsilon(2S+3S)/\Upsilon(1S)$	
	$m_g = 0\,\text{GeV/c}^2$	$m_g = 1\,\text{GeV/c}^2$
800	0.45	0.38
700	0.49	0.40
600	0.53	0.44
500	0.58	0.50

Table 1.4: Calculated ratios $\Upsilon(2S+3S)/\Upsilon(1S)$ for an effective gluon mass of 0 and $1\,\text{GeV/c}^2$ in Pb-Pb collisions at $\sqrt{s} = 2.76\,\text{TeV}$ [6].

There is a significant dependence on the QGP temperature: The higher the temperature, the bigger is the suppression of the excited states. This implies a dependence of the suppression of $\Upsilon(2S)$ and $\Upsilon(3S)$ on the center-of-mass energy $\sqrt{s}$ also in proton-proton collisions.
The CMS collaboration at LHC measured the $\Upsilon(nS)$-suppression in proton-proton collisions at a center of mass energy of $\sqrt{s} = 2.76\,\text{TeV}$ and Pb-Pb collisions at a center of mass energy of $\sqrt{s} = 2.76\,\text{TeV}$ per nucleon pair [3] [9]. The muons had transverse momenta bigger than $4\,\text{GeV/c}$ and a pseudo rapidity ($\eta = -\ln(\tan\frac{\vartheta}{2})$, where ϑ is the angle between the beam axis and the muon) between -2.4 and 2.4. For the $\Upsilon(nS)$, a cut of $p_T < 20\,\text{GeV/c}$ was applied. The observed suppression values are:

$$\begin{aligned} \frac{\Upsilon(2S+3S)}{\Upsilon(1S)}|_{pp} &= 0.78 \pm 0.18 \\ \frac{\Upsilon(2S+3S)}{\Upsilon(1S)}|_{\text{PbPb}} &= 0.24 \pm 0.15 \end{aligned} \tag{1.1}$$

One goal of this thesis is to measure this ratio in the phase space of the LHCb experiment in pp-collisions at $\sqrt{s} = 7\,\text{TeV}$ and to compare the result with the theoretical predictions in Table 1.4.

[3] It is $\sqrt{s} = 2.76\,\text{TeV}$ for the lead nuclei, because we get $2.76\,\text{TeV}/82 \cdot 208 = 7\,\text{TeV}$ per proton, which was the maximal energy of the LHC at this time.

2 LHCb Detector

LHCb is a dedicated b- and c-physics experiment at the Large Hadron Collider (LHC). The $b\bar{b}$ total cross section at $\sqrt{s} = 7\,\text{TeV}$ has been measured to be $\sim 300\,\mu\text{b}$ ($\sim 75\,\mu\text{b}$ inside the acceptance of LHCb) [3]. Fig. 2.1 shows the simulated polar angle distribution of the produced b and $\bar{b}$ quark. Due to the small angles of the b quarks with respect to the proton beams, the detector is designed as a single arm forward spectrometer and covers polar angles from $\sim 15\,\text{mrad} - 250\,\text{mrad}$. A vertical cross section through the detector is shown in Fig. 2.2. The key features of the LHCb are:

- an excellent vertex and proper time resolution;
- a precise particle identification;
- a good momentum resolution and good opening angle determination, which implies precise invariant mass resolution;
- an efficient and flexible trigger system for leptonic and hadronic final states.

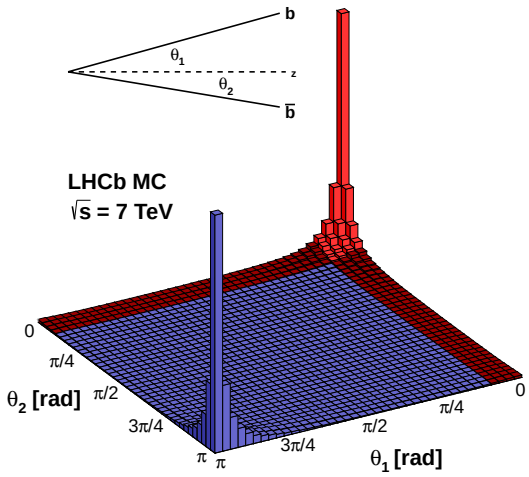

Figure 2.1: Pythia simulation of the $b\bar{b}$ cross section as a function of the polar angle of the produced b and $\bar{b}$. The bright red part corresponds to phase space with both quarks in the acceptance, the dark red to the one with only one quark.

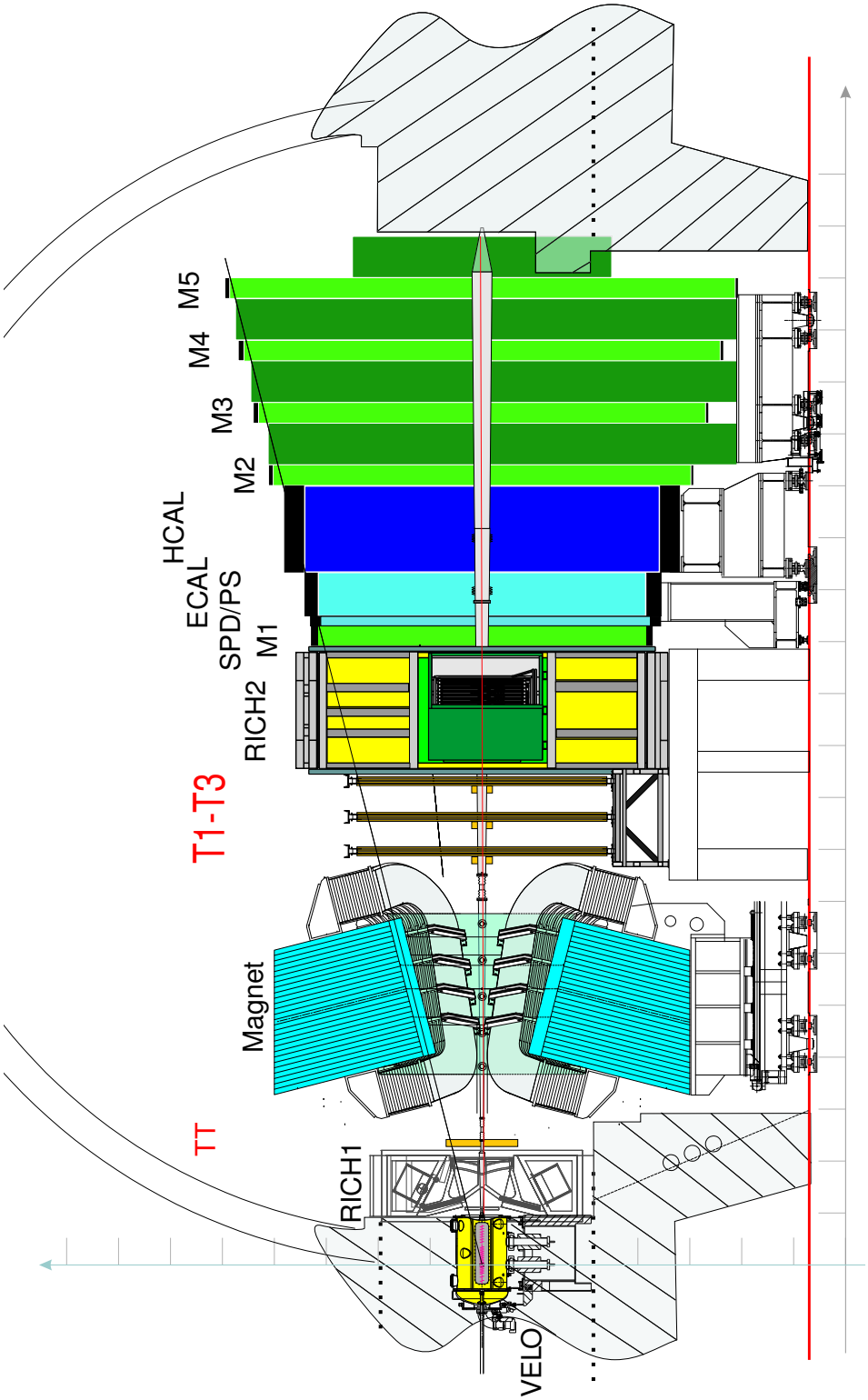

Figure 2.2: Side view of the LHCb detector showing the Vertex Locator (VELO), the dipole magnet, the two RICH detectors, the four tracking stations (TT and T1-T3), the Scintillating Pad Detector (SPD), the PreShower (PS), Electromagnetic (ECAL) and Hadronic (HCAL) calorimeteres and the Muon system (M1 - M5)

2.1 VELO and Tracking System

The tracking system consists of a dipole magnet, four tracking stations and the vertex locator (VELO). It is a silicon microstrip detector that is located at a very small distance (down to 8 mm) to the beam axis, allowing an excellent vertex resolution. For a typical event, producing 25 tracks, this resolution is 15 µm in the transverse plane and 75 µm along the beam axis.
The first tracking station (TT) is a micro-strip silicon detector. It is located upstream from the dipole magnet. The others (T1-T3) are constructed of straw tubes in the outer region, and silicon strips close to the beam pipe. They are located downstream from the magnet. The achieved relative momentum resolution is $\sigma_p/p = 0.4\%$ for $p = 1\,\mathrm{GeV/c}$ and $\sigma_p/p = 0.6\%$ for $p = 100\,\mathrm{GeV/c}$. [7], [8], [10]

2.2 Particle Identification

The two Ring Imaging Cherenkov Detectors (RICH), one upstream from the magnet, one downstream, allow to distinguish between kaons and pions up to a momentum of 100 GeV/c.
The calorimeter system consists of a pre-shower detector, a lead-scintillator Electromagnetic Calorimeter (ECAL) of shashlik type and an iron-scintillator Hadron Calorimeter (HCAL).
The muon system consists of five stations. They are equipped with Multiwire Proportional Chambers, interlaced with iron absorbers, with the exception of center of the first one, which uses triple-GEM (Gaseous Electron Multiplier) detectors.
The calorimeters and the muon system are responsible for the trigger decisions at Level 0 (Section 2.3). [7], [8], [10]

2.3 Trigger

The design luminosity of the LHCb is $2 \times 10^{32}\,\mathrm{cm^{-2}s^{-1}}$. At this luminosity, the rate of events with at least two particles in the LHCb acceptance is $\sim 10\,\mathrm{MHz}$. The trigger has to reduce this rate by a factor 2000 to 5 kHz, which is written to storage. Hence the trigger has to be highly selective and efficent. It consists of two levels: Level 0 (L0) and High Level Trigger (HLT). L0 is a hardware trigger, implemented on electronic boards. Its decision is based on calorimeter and muon chamber information and it selects muons, electrons, photons or hadrons above a given transverse momentum p_T or energy E_T. It reduces the rate to about 1 MHz. HLT is a software algorithm running on a commercial computer farm, which is separated in two stages: HLT1 uses a partial reconstruction and selects good-quality tracks. The reduction factor is about 30. HLT2 uses the fully reconstructed tracks to reduce the rate finally to 5 kHz. [7], [8], [10]

3 Analysis of Bottomonium States

3.1 Introduction

The analysis of the data taken at the LHCb experiment was performed with ROOT. Basically, we used the following formula to calculate the Bottomonium suppression ratio:

$$\gamma = \frac{N(\Upsilon(2S)) + N(\Upsilon(3S))}{N(\Upsilon(1S))} = \frac{1-f_1}{f_1} \cdot \frac{\varepsilon_{\text{trig}}(1S)}{\varepsilon_{\text{trig}}(2S+3S)} \cdot \frac{\varepsilon_{\text{sel}}(1S)}{\varepsilon_{\text{sel}}(2S+3S)} \cdot \frac{\varepsilon_{\text{rec}}(1S)}{\varepsilon_{\text{rec}}(2S+3S)} \cdot \frac{\mathcal{B}(\Upsilon(1S) \to \mu^+\mu^-)}{\mathcal{B}(\Upsilon(2S+3S) \to \mu^+\mu^-)} \tag{3.1}$$

$\frac{1-f_1}{f_1}$ is the event yield ratio, i.e. the ratio $[N(\Upsilon(2S)) + N(\Upsilon(3S))]/N(\Upsilon(1S))$, which we obtain directly from the fit. It's not yet the final value, we need to correct it with the following quantities:

- $\frac{\varepsilon_{\text{trig}}(1S)}{\varepsilon_{\text{trig}}(2S+3S)}$, the ratio of the trigger efficiencies for selected and reconstructed events,
- $\frac{\varepsilon_{\text{sel}}(1S)}{\varepsilon_{\text{sel}}(2S+3S)}$, the ratio of the selection efficiencies for reconstructed events,
- $\frac{\varepsilon_{\text{rec}}(1S)}{\varepsilon_{\text{rec}}(2S+3S)}$, the ratio of the reconstruction efficiencies and
- $\frac{\mathcal{B}(\Upsilon(1S)\to\mu^+\mu^-)}{\mathcal{B}(\Upsilon(2S+3S)\to\mu^+\mu^-)}$, the correction for the different branching fractions into $\mu^+\mu^-$ (weighted with the event yield in case of $\Upsilon(2S)$ and $\Upsilon(3S)$).

This calculation makes sure, that all possible differences in the process of data acquisition and in the analysis between the ground and the excited states are eliminated.

3.2 Data and Simulated Samples

The Monte Carlo samples are generated with Pythia6 as event generator and the decays are simulated with EvtGen. PHOTOS is used for the final state radiation simulation. With GEANT4 the detector is beeing simulated.[4]
We use a data sample from 2011 with a total integrated luminosity of $370\,\text{fb}^{-1}$. The triggerlines we used to obtain the data we are interessted in, are the following:

[4]Software versions: Reconstruction: Brunel v40r1; Trigger: Moore v12r6

Trigger	Meaning
L0Muon	$SPD \leq 600$ $p_T(\mu) \geq 1.5\,\mathrm{GeV/c}$
Hlt1DiMuonHighMass	$p_T(\mu) \geq 0.5\,\mathrm{GeV/c}$ [5] $p(\mu) \geq 6\,\mathrm{GeV/c}$ [5] $m_{\mu\mu} \geq 2.7\,\mathrm{GeV/c^2}$ IsMuon [6]
Hlt1SingleMuonHighPT	$p_T(\mu) \geq 4.8\,\mathrm{GeV/c}$ $p(\mu) \geq 8\,\mathrm{GeV/c}$ IsMuon [6]
Hlt2DiMuonB	$\frac{\chi^2}{ndof}\vert_{\text{Tracks}} \leq 5$ $\frac{\chi^2}{ndof}\vert_{\text{Primary Vertex}} \leq 10$ $m_{\mu\mu} \geq 4.7\,\mathrm{GeV/c^2}$

Table 3.1: Triggers used for the data acquisition and for the calculation of the trigger efficiency.

3.3 Selection Cuts

In order to minimise the background, we apply some additional cuts on the data sample. For both muons in each event, the following conditions have to be true:

- The χ^2 per degree of freedom ($\frac{\chi^2}{ndof}\vert_{\text{Tracks}}$) of the fit of the muon tracks has to be smaller than 4, in order to take only well reconstructed muon tracks,
- the transverse momenta (p_T) of the muons have to be bigger than 1.5 GeV/c, and
- the pseudo rapidity (η) has to be between 2 and 4.5.

For the $\Upsilon(nS)$ the pseudo rapidity has to be between 2 and 4.5, too and its momentum has to be in the range of 2 GeV/c to 500 GeV/c. The last cut is, that the $\frac{\chi^2}{ndof}\vert_{\text{Primary Vertex}}$ of the vertex fit of the reconstructed primary vertex has to be less than 20.
We apply no cuts on the impact parameters and the $\mu^+\mu^-$ vertex, because there are no hadrons which can decay to $\Upsilon(ns)$ with the exception of higher states of bottomonium.

3.4 Parameterization of Signal Mass Distribution

The mass distributions of the $\Upsilon(nS)$ signals are parameterised by a so-called "Double Crystal Ball" function (DCB), which is a Gaussian function with exponential tails to lower and higher values. The low mass tail is dominated by final state radiation, the high mass tail describes resolution effects of the detector. This function is given by:

$$f_{DCB}(m,\alpha_1,\alpha_2,n_1,n_2,\mu,\sigma) = N \cdot \begin{cases} A_1 \cdot (B_1 - \frac{m-\mu}{\sigma})^{-n_1}, & \text{for } \frac{m-\mu}{\sigma} \leq -\alpha_1 \\ \exp\left(-\frac{(m-\mu)^2}{2\sigma^2}\right), & \text{for } -\alpha_2 > \frac{m-\mu}{\sigma} > -\alpha_1 \\ A_2 \cdot (B_2 - \frac{m-\mu}{\sigma})^{-n_2}, & \text{for } \frac{m-\mu}{\sigma} \geq -\alpha_2 \end{cases} \tag{3.2}$$

[5] for both muons
[6] A particle is called "IsMuon", if there is a certain number of muon station hits in a Field of Interest defined by the track extrapolation. The number of required hits is momentum dependent.

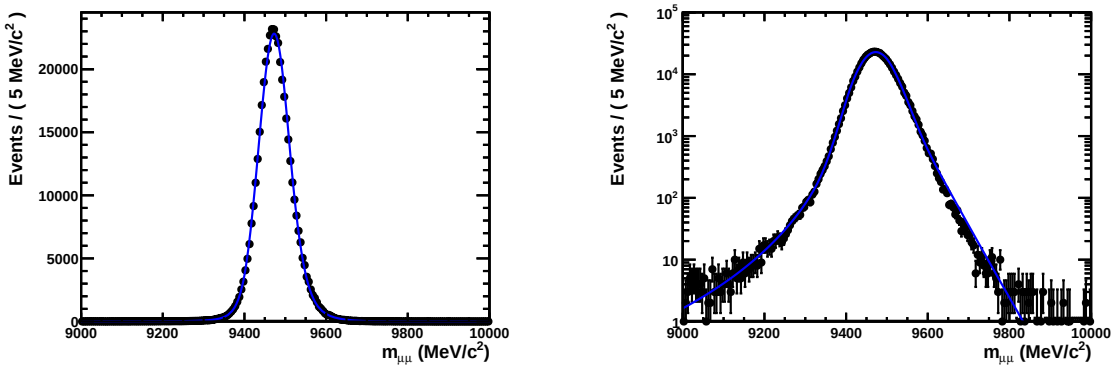

Figure 3.1: Fit of a DCB function to the $\Upsilon(1S)$-signal of a simulated data sample without background (linear and logarithmic plots).

$$\text{where } A_{1,2} = \left(\frac{n_{1,2}}{|\alpha_{1,2}|}\right)^{n_{1,2}} \cdot \exp\left(-\frac{|\alpha_{1,2}|^2}{2}\right) \text{ and } B_{1,2} = \frac{n_{1,2}}{|\alpha_{1,2}|} - |\alpha_{1,2}|$$

Where μ and σ are the mean and standard deviation of the Gaussian, α_1 is the distance in standard deviations from the peak to the start of the low mass tail, α_2 the distance to the beginning of the high mass tail and n_1 and n_2 are the exponents of the power function of the tails.
Because it is difficult to fit the parameters describing these mass tails (α and n) on top of background, we determine them from simulated event samples and fix them in the fit to the data. Their value is obtained from a fit of a DCB function to the invariant dimuon mass from a sample of simulated $\Upsilon(1S) \to \mu^+\mu^-$ events and is taken the same for all $\Upsilon(nS)$-peaks (Fig. 3.1). The selection cuts described in Section 3.3 are also used for the simulation sample in order to be consistent. The obtained values from the fit, shown in Fig. 3.1, are: $\alpha_1 = 1.864 \pm 0.016$, $\alpha_2 = -1.072 \pm 0.006$, $n_1 = 4.03 \pm 0.12$ and $n_2 = 142 \pm 29$.

3.5 Fit

The complete fit function for the data is the sum of 3 DCB functions for the three $\Upsilon(nS)$-resonances and an exponential distribution for the background:

$$\begin{aligned} f(m) =& (1 - f_{BKG})\{f_1 \cdot f_{DCB,\Upsilon(1S)} + (1 - f_1)(f_2 \cdot f_{DCB,\Upsilon(2S)} \\ &+ (1 - f_2) \cdot f_{DCB,\Upsilon(3S)})\} + f_{BKG} \cdot \exp(-\lambda \cdot m) \end{aligned} \tag{3.3}$$

There are ten parameters that have to be fitted: Two per DCB function (the mean ($\Upsilon(nS)$-masses) and the standard deviations), three fraction factors (f_{BKG}, f_1, f_2) and the λ for the background. The used RooFit tool uses the Maximum Likelihood method for the fit.

The values of the fit parameters are summarized in Table 3.2.

Parameter	$\mu_{\Upsilon(1S)}$	$\mu_{\Upsilon(2S)}$	$\mu_{\Upsilon(3S)}$
Value	$(9440.2 \pm 0.1)\,\mathrm{MeV/c^2}$	$(10\,002.2 \pm 0.3)\,\mathrm{MeV/c^2}$	$(10\,333.1 \pm 0.5)\,\mathrm{MeV/c^2}$
Parameter	$\sigma_{\Upsilon(1S)}$	$\sigma_{\Upsilon(2S)}$	$\sigma_{\Upsilon(3S)}$
Value	$(44.1 \pm 0.1)\,\mathrm{MeV/c^2}$	$(47.1 \pm 0.3)\,\mathrm{MeV/c^2}$	$(49.7 \pm 0.5)\,\mathrm{MeV/c^2}$

Table 3.2: Means and standard deviations of the Gaussian parts of the fit function.

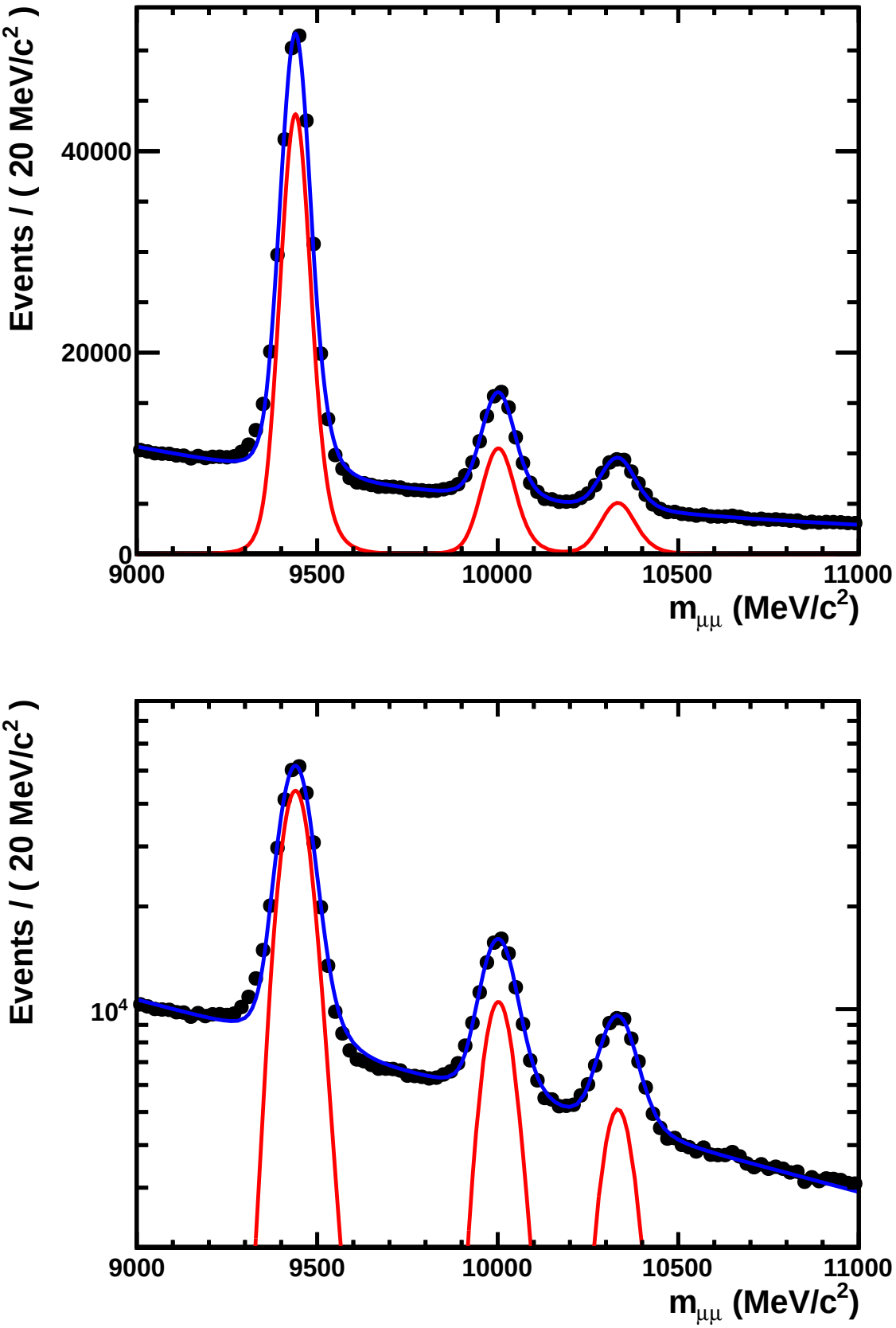

Figure 3.2: Fit of $\mu^+\mu^-$ invariant mass distribution to data (black points) at $\sqrt{s} = 7\,\text{TeV}$. The blue line is the total fit, the red lines are the DCB functions for the three $\Upsilon(nS)$-states without background (linear and logarithmic plots).

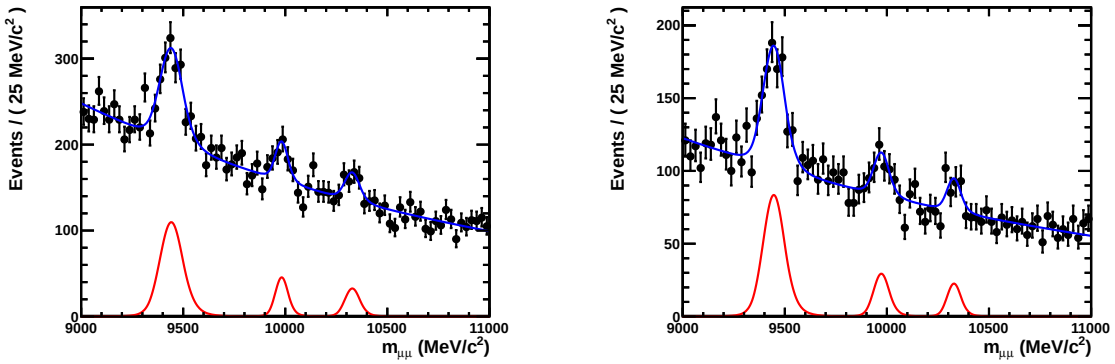

Figure 3.3: Left side: only TIS events; Right side: TIS & TOS events; and the fitted distributions as above.

The means μ of the DCB disagree with the $\Upsilon(nS)$ masses quoted in Table 1.2, due to an overestimation of the muon momenta by the LHCb detector, which already has been observed in other analyses [4]. f_2 is the fraction of $\Upsilon(2S)$ in $\Upsilon(2S{+}3S)$ and the fit yields $f_2 = 0.6646{\pm}0.0026$. We use this factor for the weighting of the branching fractions of $\Upsilon(2S)$ and $\Upsilon(3S)$ in the correction for the different branching fractions to $\mu^+\mu^-$, because we analyse the excited states together. In Sections 3.7 to 3.9 we have separate simulated samples for $\Upsilon(2S)$ and $\Upsilon(3S)$. In order to obtain a simulated sample of the excited states together, we use f_2 for the weighting of the histograms in the summation.
The most important value is the event yield ratio $\frac{1-f_1}{f_1}$ between $\Upsilon(1S)$ and $\Upsilon(2S)$, $\Upsilon(3S)$. This value (and f_2 as well) is not affected by the disagreement in the $\Upsilon(nS)$-masses.

$$\frac{1-f_1}{f_1} = 0.392 \pm 0.003 \tag{3.4}$$

3.6 Trigger Efficiency

We use the TIS TOS method for the trigger efficiency calculation and analyse the trigger efficency separately for the $\Upsilon(1S)$ and for the $\Upsilon(2S+3S)$.
An event is classified as TOS (Trigger On Signal), if our signal object (i.e. dimuon system) has fired all trigger levels, regarding the considered lines listed in Table 3.1. An event is classified as TIS (Trigger Independent of Signal), if there is another object than our signal object that has fired all trigger levels.
We can calculate the trigger efficency $\varepsilon_{\text{trig}}$ by dividing the number of events, which are classified as TIS and TOS by the number of events, which are classified as TIS. These numbers of events are calculated as a simple integration of the fit functions (Fig. 3.3). This method should lead to a data driven estimation of the trigger efficiency. The result for the ground state $\Upsilon(1S)$ is:

$$\varepsilon_{\text{trig}}(1S) = 0.715 \pm 0.013 \tag{3.5}$$

for the excited states $\Upsilon(2S+3S)$ it is:

$$\varepsilon_{\text{trig}}(2S+3S) = 0.721 \pm 0.029 \tag{3.6}$$

and the ratio of these two is:

$$\frac{\varepsilon_{\text{trig}}(1S)}{\varepsilon_{\text{trig}}(2S+3S)} = 0.99 \pm 0.04 \tag{3.7}$$

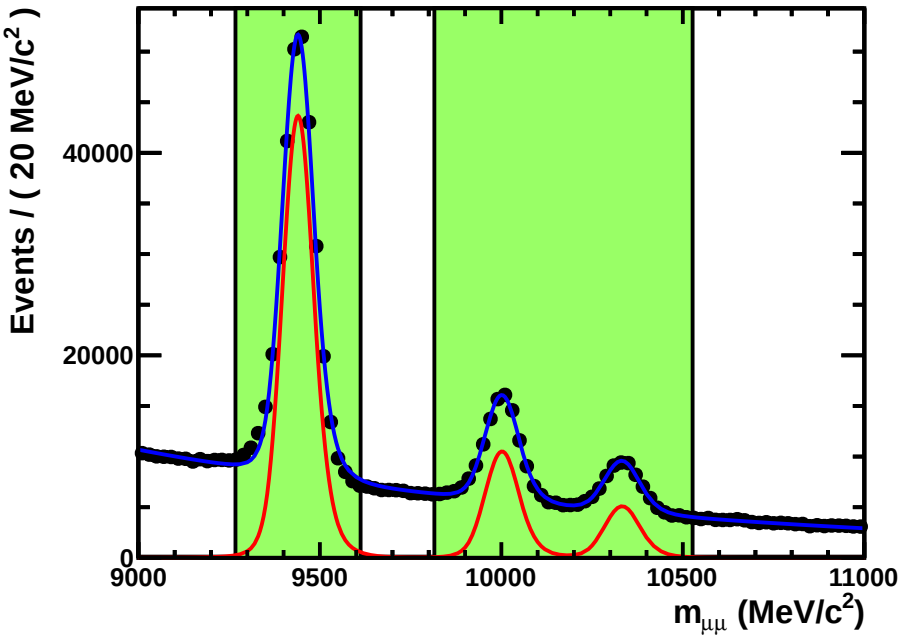

Figure 3.4: Green region: $\pm 4\sigma$ around the mass peaks defined as signal window; white region: sidebands

The ratio of the two trigger efficencies is consistent with 1. The statistical uncertainty on the efficiency ratio will be assigned to the systematic uncertainty on the final result.

3.7 Sideband Subtraction

We use a sideband subtraction method to obtain the distribution of a certain variable for signal events. We can use these distributions to check differences between $\Upsilon(1S)$ and $\Upsilon(2S+3S)$ or between data and Monte Carlo.
First we calculate the number of events in a range of $\pm 4\sigma$ around the $\Upsilon(1S)$ signal or the excited states (Fig. 3.4), this is an easy integration of the fitted function. In the same range, we then calculate the number of background events, and the number of signal events, again by integration of the background exponential function and the DCB function for the signals. We assume the background events above and below the signals (the sidebands, white region in Fig. 3.4) to have the same distribution of the variables as the background events under the signals. So, we take the distributions of the variables for events in the sidebandes, normalise them and multiply them with the number of background events in the $\pm 4\sigma$ region around the signals. This generates the distribution of the variable for the background events under the signals. If we subtract the background distribution of the entire distribution of the range around the signals, we get the distribution of the variable for signal events only.
We execute this technique for the $\Upsilon(1S)$ ground state and treat the $\Upsilon(2S)$ and $\Upsilon(3S)$ excited states together as usual. We use this method to compare distributions between $\Upsilon(1S)$ and $\Upsilon(2S+3S)$ (Fig. 3.5), as well as to compare distributions from data and Monte Carlo (Fig. 3.6 and Fig. 3.7). The variables, which are used for the comparison between the ground and the excited states, are:

- Number of Long Tracks: The tracks which are reconstructed in the VELO, TT and T1-T3
- $p_T(\Upsilon(nS))$, $p_T(\mu^-)$, $p_T(\mu^+)$: The transverse momenta of the mother particle ($\Upsilon(nS)$), the positive and the negative charged muon
- $\eta(\mu^-)$, $\eta(\mu^+)$: The pseudorapidities of the muons

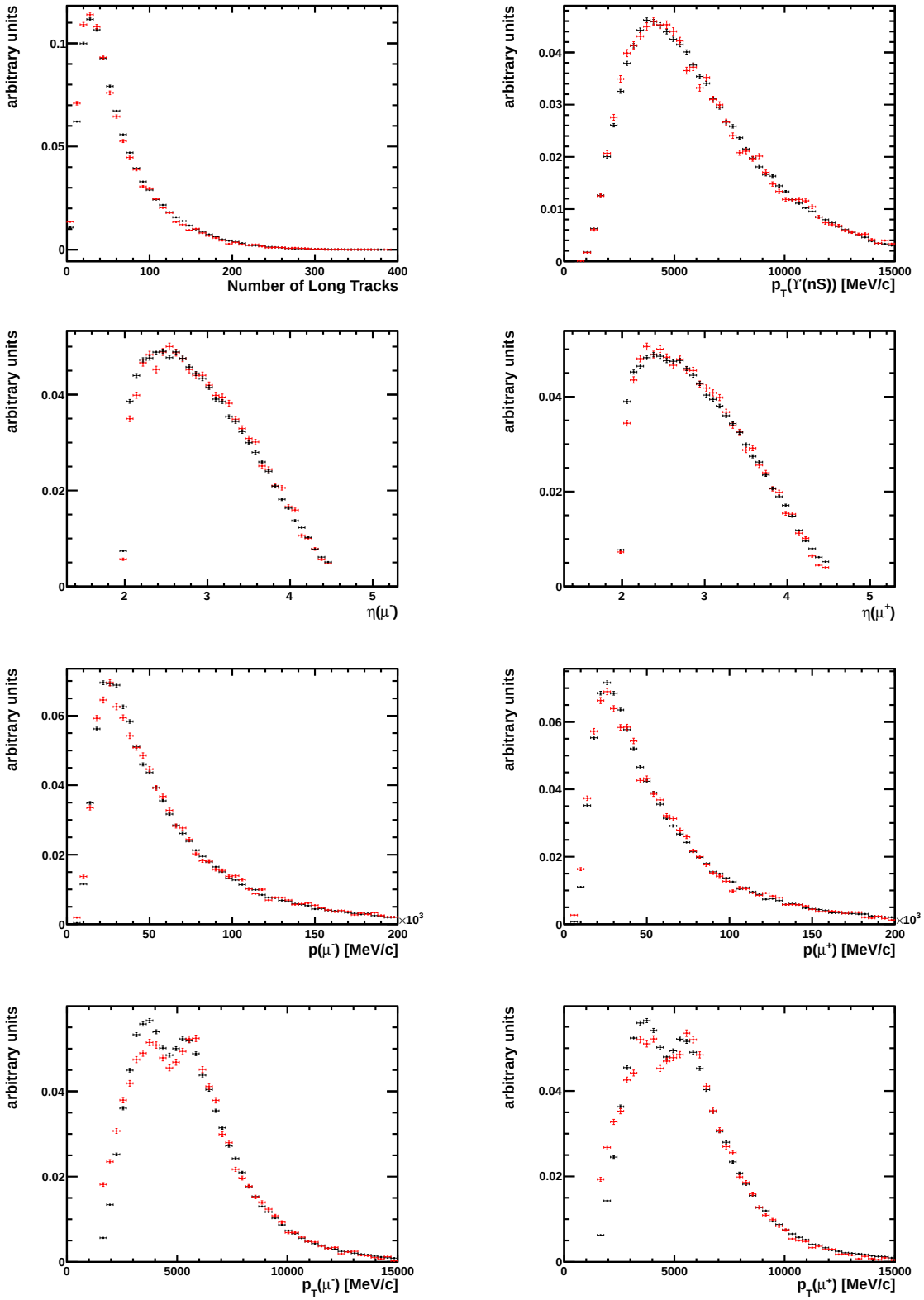

Figure 3.5: Normalized, sideband subtracted distributions for $\Upsilon(1S)$ (black) in comparison with $\Upsilon(2S+3S)$ (red).

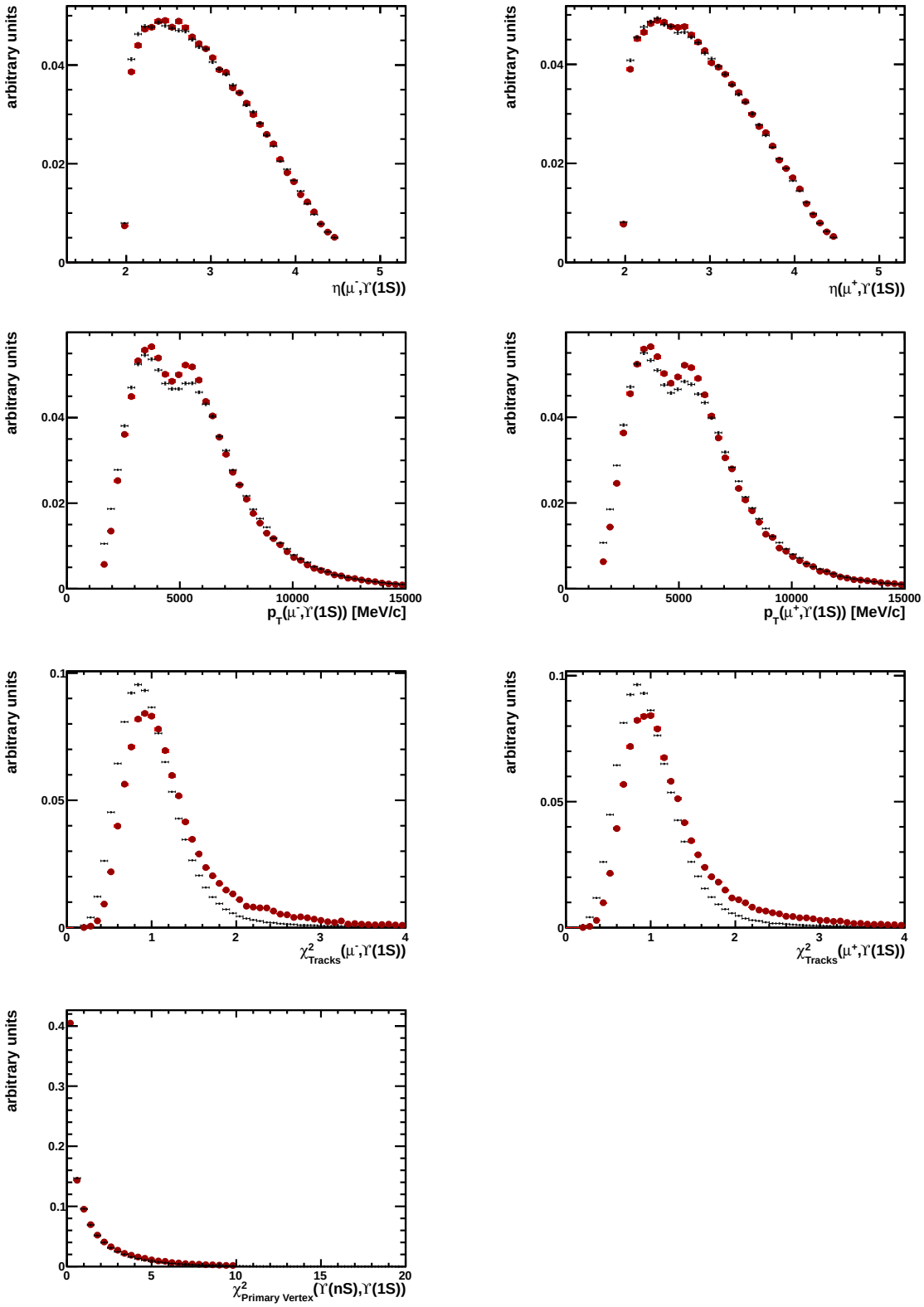

Figure 3.6: Comparison of the data (red) and Monte Carlo samples (black) for $\Upsilon(1S)$. The axis label means: e.g. $p_T(\mu^-, \Upsilon(1S))$: the (sideband subtracted) variable p_T of the particle μ^- for events in the $\Upsilon(1S)$ signal region.

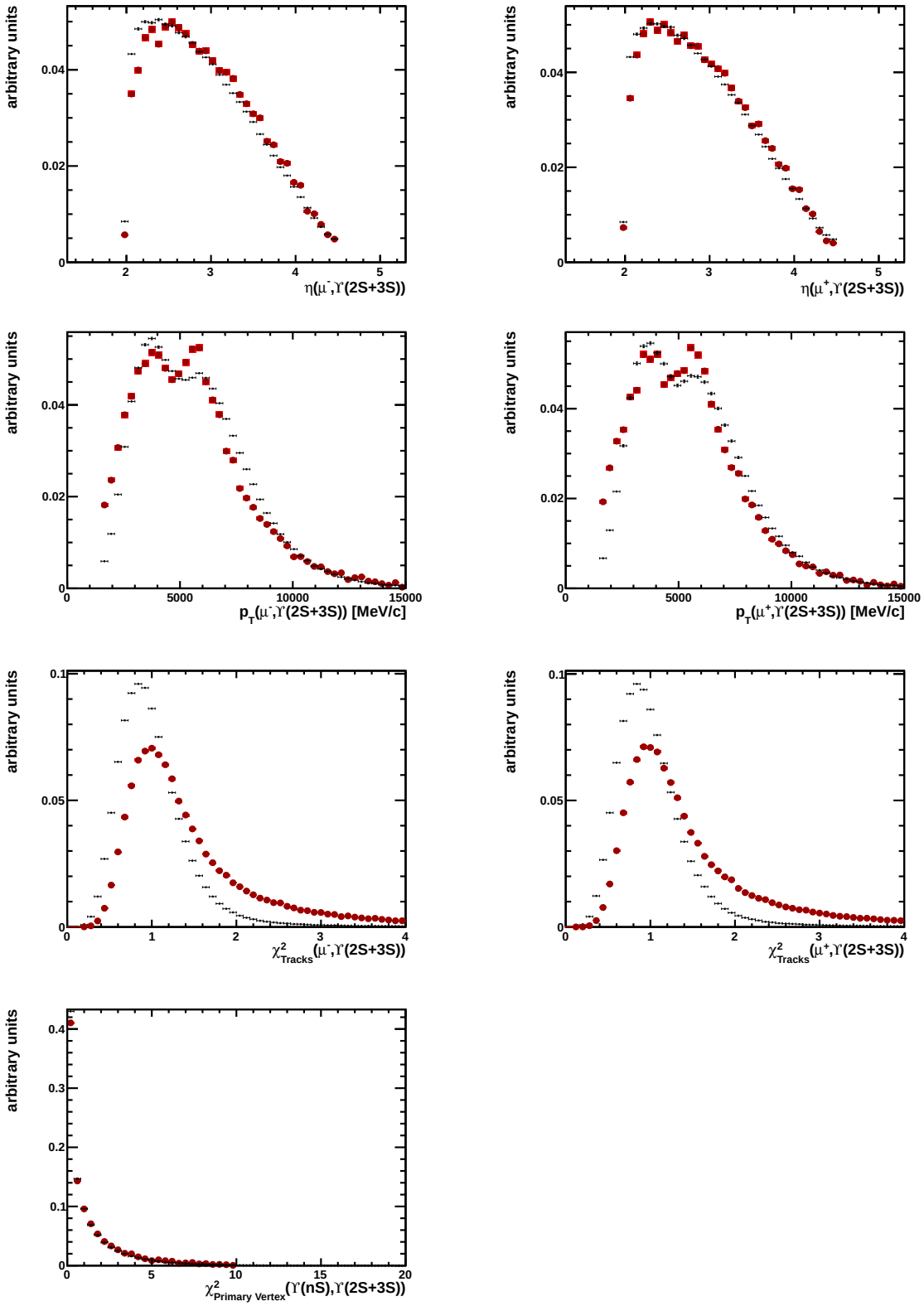

Figure 3.7: Comparison of the data (red) and Monte Carlo samples (black) for $\Upsilon(2S+3S)$. We use the same notation as in Fig. 3.6.

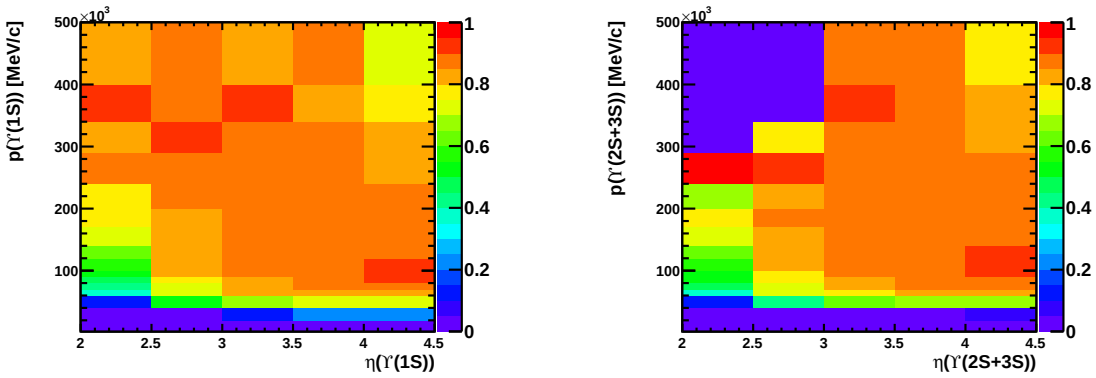

Figure 3.8: Selection efficiency for $\Upsilon(1S)$ (left) and $\Upsilon(2S+3S)$ (right).

- $p_(\mu^-)$, $p_(\mu^+)$: The momenta of the muons

The distributions of the variables are mostly consistent with each other within the uncertainties (Fig. 3.4). This means the efficiency of the selection cuts for the excited and for the ground states is comparable with each other.
In order to make sure that the Monte Carlo generated samples are consistent with the data samples, we also compare the sideband-subtracted distributions of the variables which are used in the selection cuts with the distributions of the same variables of the simulated samples, again for the $\Upsilon(1S)$ (Fig. 3.6) ground state and for the $\Upsilon(2S+3S)$ (Fig. 3.7) excited states separately. The variables we use, are (each for the $\Upsilon(1S)$ and the $\Upsilon(2S+3S)$):

- $\eta(\mu^-)$, $\eta(\mu^+)$: The pseudorapidities of the muons
- $p_T(\mu^-)$, $p_T(\mu^+)$: The transverse momenta of the muons
- $\frac{\chi^2}{ndof}|_{\text{Tracks}}$: The χ^2 per degree of freedom of the reconstructed muon tracks
- $\frac{\chi^2}{ndof}|_{\text{Primary Vertex}}$ The χ^2 per degree of freedom of the primary vertex of the $\Upsilon(nS)$

The data and Monte Carlo distributions of the different variables are mostly consistent with each other within the uncertainties. The only differences between the two are in $\frac{\chi^2}{ndof}|_{\text{Tracks}}$. The reason is a slightly different reconstruction in the Monte Carlo sample, because we use a Monte Carlo sample from 2012.

3.8 Selection Efficiency

The selection efficiency is defined as the fraction of signal events that passed our selection cuts. For the calculation, we use the Monte Carlo samples. First, we fill a two-dimensional histogram in pseudo rapidity (5 bins) and momentum (16 bins) with the Monte Carlo generated data. Then we apply the selection cuts and fill a second histogram with the selected events. If we take the ratio of the two histograms, we obtain the selection efficiency for each bin of the histogram for the ground state and the excited states seperately (Fig. 3.8).

To calculate the overall selection efficiency, we weight each bin with the number of data events it contains. So we fill the same two-dimentional histogram with the sideband-subtracted data and normalize it (Fig. 3.9). Integration of the weighted histograms resuls in the average selection efficiency. For $\Upsilon(1S)$ it is:

$$\varepsilon_{\text{sel}}(1S) = 0.833 \pm 0.003 \tag{3.8}$$

for $\Upsilon(2S+3S)$ it is:

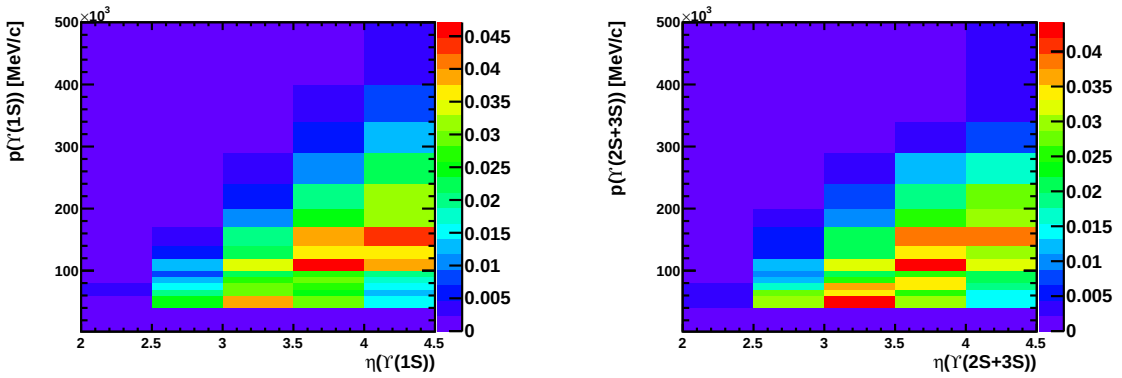

Figure 3.9: Normalized distribution of the data events for $\Upsilon(1S)$ (left) and $\Upsilon(2S+3S)$ (right) in η and p.

$$\varepsilon_{\text{sel}}(2S+3S) = 0.820 \pm 0.006 \tag{3.9}$$

and the ratio is:

$$\frac{\varepsilon_{\text{sel}}(1S)}{\varepsilon_{\text{sel}}(2S+3S)} = 1.016 \pm 0.008 \tag{3.10}$$

Here we assume the uncertainties on $\varepsilon_{\text{sel}}(1S)$ and $\varepsilon_{\text{sel}}(2S+3S)$ to be uncorrelated and use the simple error propagation to calculate the uncertainty on the ratio. We find no large difference between ground and excited states in the selection efficiency. The statistical uncertainty on the efficiency ratio will be assigned to the systematic uncertainty on the final result.

3.9 Reconstruction Efficiency

The reconstruction efficiency is defined as the fraction of $\Upsilon(nS)$ with pseudo rapidity in the range of 2-4.5 and momentum between 2 GeV/c and 500 GeV/c, where both muons are in the LHCb acceptance and are reconstructed. We calculate it very similarly to the selection efficiency and use the simulated data samples as well. First we fill the Monte Carlo sample on generator level in a two-dimensional histogram in η (5 bins) and p (16 bins). Then, we fill a second histogram, but we require the $\Upsilon(nS)$ to be identified as reconstructed [7]. The ratio of the two histograms gives the reconstruction efficiency (Fig. 3.10) in bins of p and η. We weight with the number of signal events per bin (Fig. 3.9) as in the determination of the selection efficiency and integrate it to obtain the average reconstruction efficiency. For $\Upsilon(1S)$ the result is:

$$\varepsilon_{\text{rec}}(1S) = 0.2711 \pm 0.0012 \tag{3.11}$$

for $\Upsilon(2S+3S)$ it is:

$$\varepsilon_{\text{rec}}(2S+3S) = 0.2692 \pm 0.0020 \tag{3.12}$$

and the ratio is:

$$\frac{\varepsilon_{\text{rec}}(1S)}{\varepsilon_{\text{rec}}(2S+3S)} = 1.007 \pm 0.008 \tag{3.13}$$

[7] The classification as reconstructed is done by measuring the overlap between the simulated tracks and the reconstructed tracks of the muons.

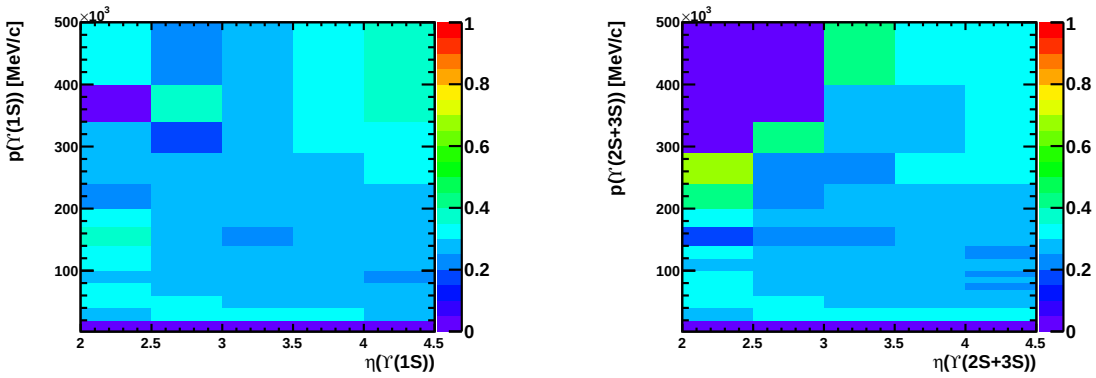

Figure 3.10: Reconstruction efficiencies for $\Upsilon(1S)$ and $\Upsilon(2S+3S)$.

The uncertainties are assumed to be uncorrelated and the uncertainty on the ratio is determined by simple error propagation. The ratio of the reconstruction efficiencies is consistent with 1 within the uncertainty. The statistical uncertainty on the efficiency ratio will be assigned as a systematic uncertainty on the final result.

3.10 Final result

We combine all previous results to our final result using Eq. (3.1). We obtain for the bottomonium-suppression in the phase space of the $\Upsilon(nS)$ of $2.0 \leq \eta \leq 4.5$ and $2\,\mathrm{GeV/c} \leq p \leq 500\,\mathrm{GeV/c}$:

$$\gamma = \frac{\Upsilon(2S+3S)}{\Upsilon(1S)} = 0.489 \pm 0.004_{\mathrm{stat}} \pm 0.021_{\mathrm{sys}} \pm 0.034_{\mathcal{B}} \tag{3.14}$$

The statistical uncertainty comes from the event yield. The uncertainties of the trigger, selection and reconstruction efficiency are added in quadrature to the systematical uncertainty and the last uncertainty is a consequence of the uncertainties of the $\Upsilon(nS) \to \mu^+\mu^-$ branching fractions quoted in Table 1.2. The suppression factor includes $\Upsilon(nS)$ mesons which have been decay products of other bottomonium states, like in the decay $\chi_{b0} \to \Upsilon(1S)\gamma$. We have not corrected for those decays.

4 Analysis of Charmonium States

4.1 Introduction

The analysis of the $J/\psi(1S)$ and $\psi(2S)$ is basically the same as the analysis of the $\Upsilon(nS)$-states. We use the following formula to calculate the final result:

$$\begin{aligned}\gamma = \frac{N(\psi(2S))}{N(J/\psi(1S))} =& \frac{1-f_1}{f_1} \cdot \frac{\varepsilon_{\text{trig}}(1S)}{\varepsilon_{\text{trig}}(2S)} \cdot \frac{\varepsilon_{\text{sel}}(1S)}{\varepsilon_{\text{sel}}(2S)} \cdot \frac{\varepsilon_{\text{rec}}(1S)}{\varepsilon_{\text{rec}}(2S)} \\ & \cdot \frac{\mathcal{B}(J/\psi(1S) \to \mu^+\mu^-)}{\mathcal{B}(\psi(2S) \to \mu^+\mu^-)} \cdot \frac{f_{\text{prompt}}(\psi(2S))}{f_{\text{prompt}}(J/\psi(1S))}\end{aligned} \tag{4.1}$$

It is the same formula as for the Bottomonium (Eq. (3.1)) except for the additional factor $\frac{f_{prompt}(\psi(2S))}{f_{prompt}(J/\psi(1S))}$, correcting for the fact that we are only interested in prompt charmonium production and not in charmonium originating from B decays.

4.2 Data and Monte Carlo Samples

We use a data sample from 2011 with an integrated luminosity of $370\,\text{fb}^{-1}$. The event yields are relatively small due to a significant prescale in the trigger. The simulated events are generated with Pythia6 as an event generator and the decays are simulated with EvtGen. PHOTOS is used for the final state radiation simulation. With GEANT4 the detector is beeing simulated.[8]

4.3 Selection cuts

The selection cuts are the same as for the $\Upsilon(nS)$-states (Section 3.3). There is one additional cut: The transverse momentum of the mother particle must be smaller than $14\,\text{GeV/c}$. This cut is introduced to be able to use the ratio of prompt $J/\psi(1S)$ and $\psi(2S)$ measured in [1] and [2] (see Section 4.10).
We apply no cuts on the impact parameters and the $\mu^+\mu^-$ vertex, because we correct for the fraction of prompt charmonium products (Section 4.10).

4.4 Parameterization of Signal Mass Distribution

The mass distribution for signal events for $\psi(nS)$ are parameterised by a DCB function (Eq. (3.2)). The tail parameters are fixed in the fit to data for the same reasons as in Section 3.4. These values come from a simulated sample of $J/\psi(1S) \to \mu^+\mu^-$ events (Fig. 4.1). They are: $\alpha_1 = 1.821 \pm 0.007$; $\alpha_2 = -1.098 \pm 0.003$; $n_1 = 3.93 \pm 0.05$ and $n_2 = 139.016 \pm 0.005$.

[8] Software versions: Reconstruction: Brunel v40r1; Trigger: Moore v12r6

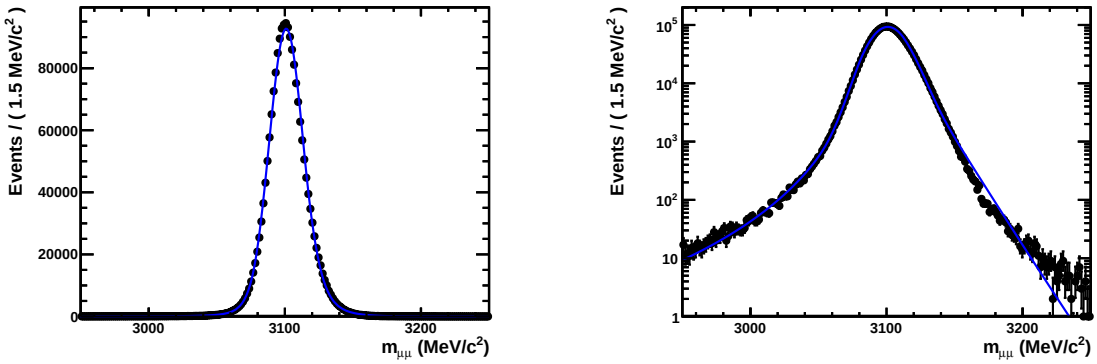

Figure 4.1: Fit of a DCB function to a $J/\psi(1S)$-peak of a Monte Carlo generated data sample without background (linear and logarithmic plots).

4.5 Fit

The complete fit function of the data is the sum of two DCB functions for the signals and an exponential function to describe background:

$$f(x) = (1 - f_{BKG})\{f_1 \cdot f_{DCB,J/\psi(1S)} + (1 - f_1) \cdot f_{DCB,\psi(2S)}\} + f_{BKG} \cdot \exp(-\lambda \cdot x) \qquad (4.2)$$

Seven parameters have to be fitted: Two per DCB function (the mean and the standard deviation), two fraction factors and the exponential background parameter. The result of the fit is shown in Fig. 4.2, the results for the means and standard deviations are listed in Table 4.1.

Parameter	$\mu_{J/\psi(1S)}$	$\mu_{\psi(2S)}$
Value	$(3091.34 \pm 0.09)\,\mathrm{MeV/c^2}$	$(3677.0 \pm 1.2)\,\mathrm{MeV/c^2}$
Parameter	$\sigma_{J/\psi(1S)}$	$\sigma_{\psi(2S)}$
Value	$(12.96 \pm 0.08)\,\mathrm{MeV/c^2}$	$(16.3 \pm 1.2)\,\mathrm{MeV/c^2}$

Table 4.1: Charmonia-masses and standard deviations.

The relative deviation between the measured means and the nominal masses of the resonances quoted in the PDG [5] is as in case of the $\Upsilon(nS)$ resonances about 0.2%. The fit yields an event yield ratio at $\sqrt{s} = 7\,\mathrm{TeV}$ of:

$$\frac{1 - f_1}{f_1} = 0.0345 \pm 0.0025 \qquad (4.3)$$

4.6 Trigger Efficiency

For L0 and HLT1 we assume a similar efficiency due to results from previous analyses [11], [12]. For HLT2, we analyse the trigger efficiency separately for the ground state and the excited state. We use the TIS TOS method for the trigger efficiency calculation. It is described in detail in Section 3.6.
The trigger line in Table 4.2 is used for the analysis of the HLT2.

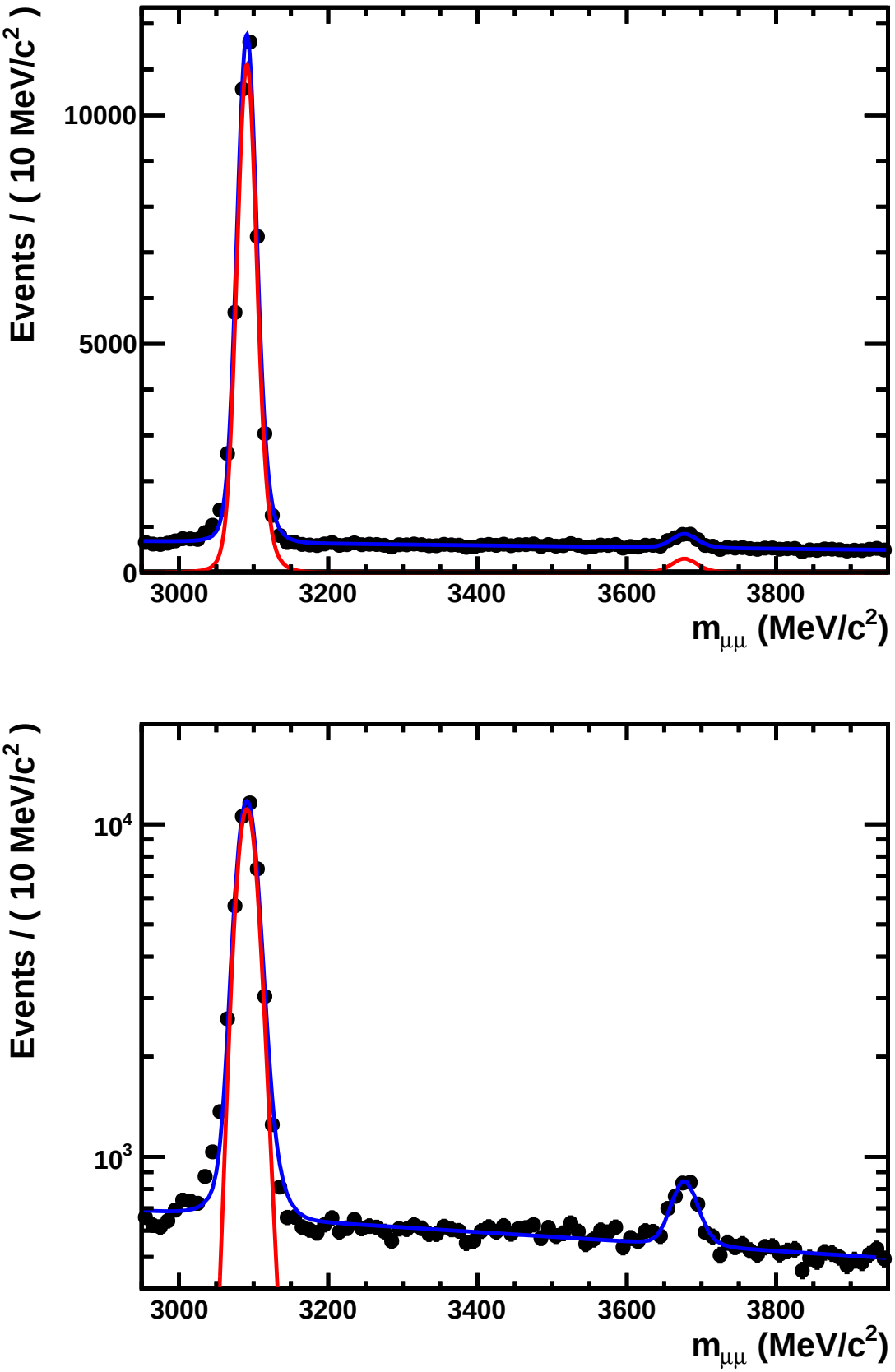

Figure 4.2: Fit of the $J/\psi(1S)$ ground state and the $\psi(2S)$ excited state for data (black points) at $\sqrt{s} = 7\,\text{TeV}$. The blue line is the total fit, the red lines are the DCB functions for the $J/\psi(1S)$ and the $\psi(2S)$ signals (linear and logarithmic plots).

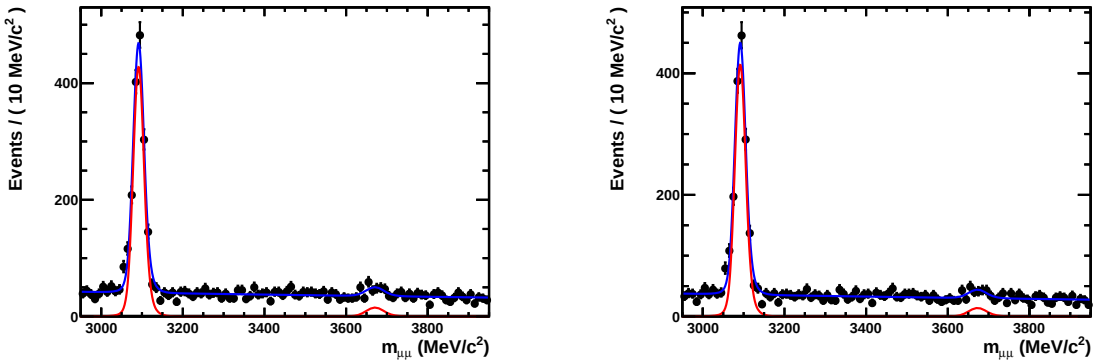

Figure 4.3: Left side: only TIS events on HLT2 level; Right side: TIS & TOS events on HLT2 level; and the fitted distributions as above.

Trigger	Meaning
Hlt2DiMuonLowMass	$\frac{\chi^2}{ndof}\vert_{\text{Tracks}} \leq 5$ $\frac{\chi^2}{ndof}\vert_{\text{Primary Vertex}} \leq 25$ $m_{\mu\mu} \geq 0.5\,\text{GeV/c}^2$

Table 4.2: Trigger used for the calculation of the trigger efficiency on HLT2 level.

The result for the $J/\psi(1S)$ is:

$$\varepsilon_{\text{trig}}(1S) = 0.9685 \pm 0.0023 \tag{4.4}$$

for the $\psi(2S)$ it is:

$$\varepsilon_{\text{trig}}(2S) = 0.92 \pm 0.12 \tag{4.5}$$

and the ratio of these two is:

$$\frac{\varepsilon_{\text{trig}}(1S)}{\varepsilon_{\text{trig}}(2S)} = 1.05 \pm 0.08 \tag{4.6}$$

This value is consistent with 1. The statistical uncertainty on the efficiency ratio will be assigned as a systematic uncertainty on the final result.

4.7 Sideband Subtraction

The sideband subraction is exactly the same as for the bottomonium (Section 3.7). We use a signal range of $\pm 4\sigma$ around the signals, for the sidebands we choose a width of 8σ on both sides adjacent to the signal window (Fig. 4.4).

We compare the distribution of the following variables (Fig. 4.4):

- Number of Long Tracks: The tracks which are detected in the VELO, TT and T1-T3,
- $p_T(\psi(nS))$, $p_T(\mu^-)$, $p_T(\mu^+)$: The transverse momenta of the mother particle ($\psi(nS)$), the positive and the negative charged muon,
- $\eta(\mu^-)$, $\eta(\mu^+)$: The pseudorapidities of the muons, and

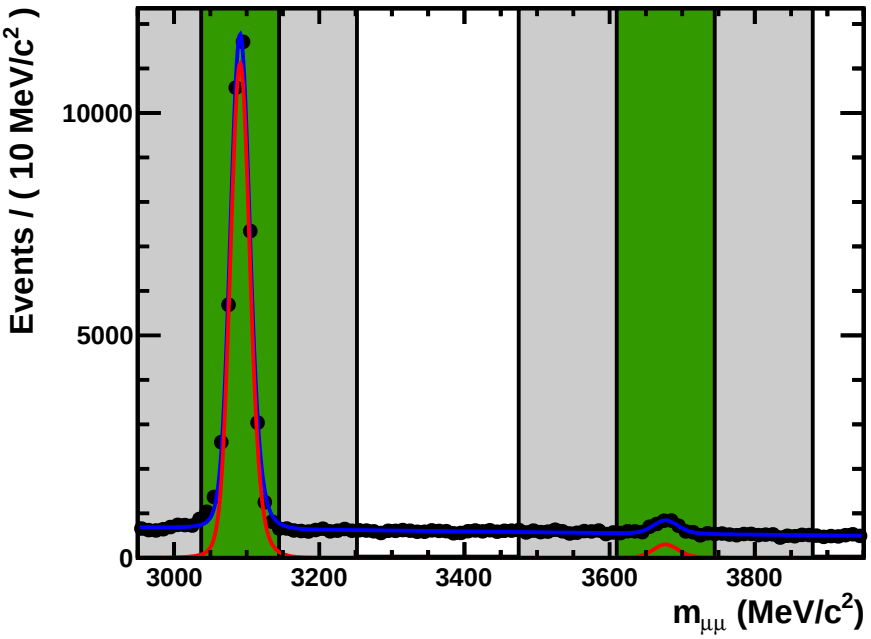

Figure 4.4: Green region: $\pm 4\sigma$ around the mass peaks defined as signal window; gray region: sidebands

- $p_(\mu^-)$, $p_(\mu^+)$: The momenta of the muons.

The two distributions are consistent within the uncertainties, but we can see effects of low statistics in the distributions for $\psi(2S)$.
We also compare the simulated samples with our data for the $J/\psi(1S)$ (Fig. 4.6) and the $\psi(2S)$ (Fig. 4.7) seperately. The variables we use are (each for the $J/\psi(1S)$ and the $\psi(2S)$):

- $\eta(\mu^-)$, $\eta(\mu^+)$: The pseudo rapidities of the muons,
- $p_T(\mu^-)$, $p_T(\mu^+)$: The transverse momenta of the muons,
- $\frac{\chi^2}{ndof}|_{\text{Tracks}}$: The χ^2 per degree of freedom of the reconstructed muon tracks, and
- $\frac{\chi^2}{ndof}|_{\text{Primary Vertex}}$: The χ^2 per degree of freedom of the primary vertex of the $\psi(nS)$.

The data and Monte Carlo distributions of the different variables are consistent with each other within the uncertainties. The only differences between the two are in $\frac{\chi^2}{ndof}|_{\text{Tracks}}$. The reason is a slightly different reconstruction in the Monte Carlo sample, because we use a Monte Carlo sample from 2012.

4.8 Selection Efficiency

The selection efficiency is calculated in the same manner as for the bottomonia (Section 3.8). The binned histograms in η (5 bins) and p (16 bins) of the calculated selection efficiency are shown in Fig. 4.8.

The normalized histograms for the weighting of the selection and reconstruction efficiency with the number of data events in each bin are shown in Fig. 4.9. The resulting selection efficiency for $J/\psi(1S)$ is:

$$\varepsilon_{\text{sel}}(1S) = 0.3920 \pm 0.0024 \tag{4.7}$$

for $\psi(2S)$ it is:

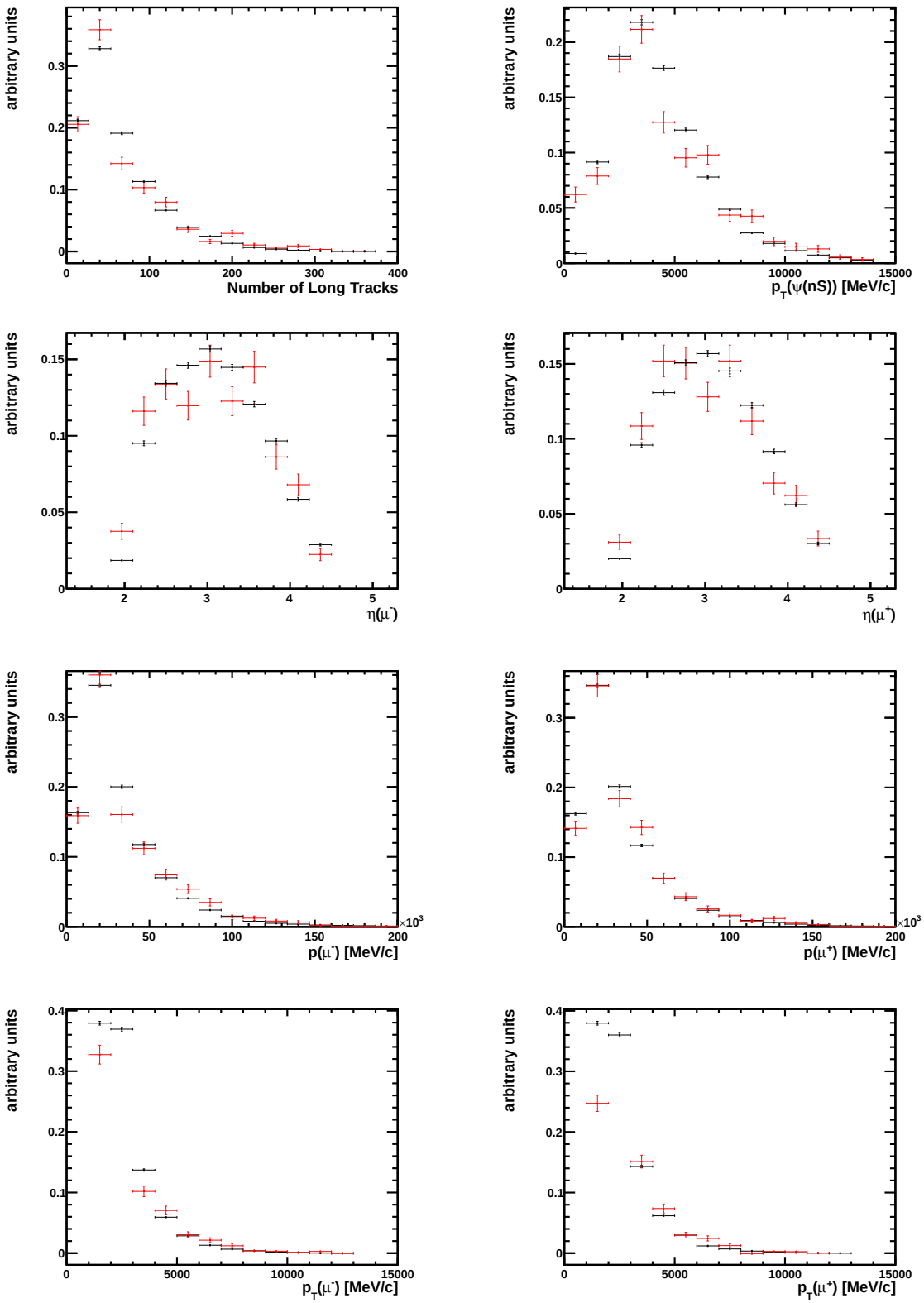

Figure 4.5: Normalized, sideband subtracted distributions of $J/\psi(1S)$ (black) in comparison with $\psi(2S)$ (red).

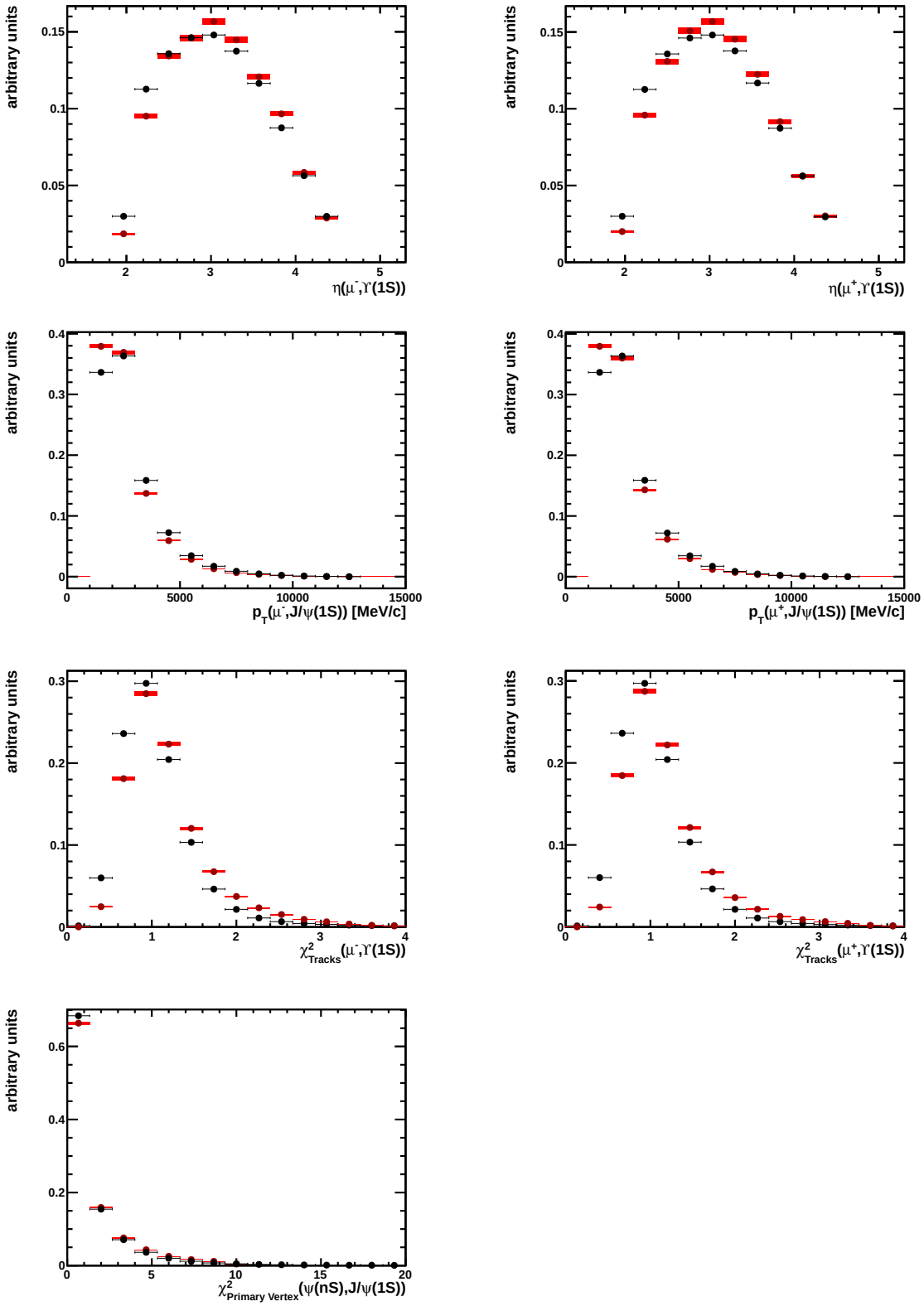

Figure 4.6: Comparison of data (black lines) and simulated samples (red dots) for $J/\psi(1S)$. We use the same notation as in Fig. 3.6.

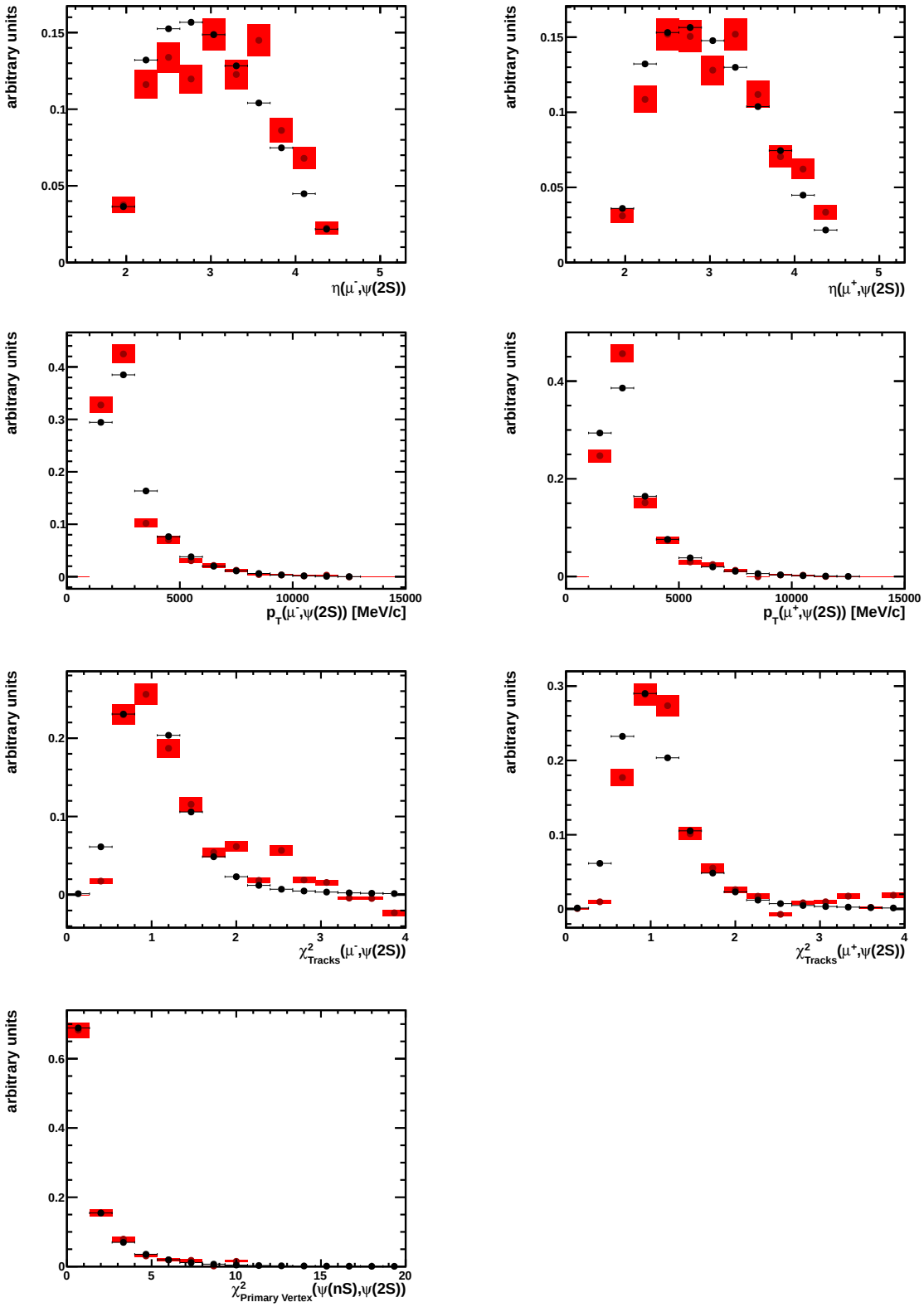

Figure 4.7: Comparison of data (black lines) and simulated samples (red dots) for $\psi(2S)$. We use the same notation as in Fig. 3.6.

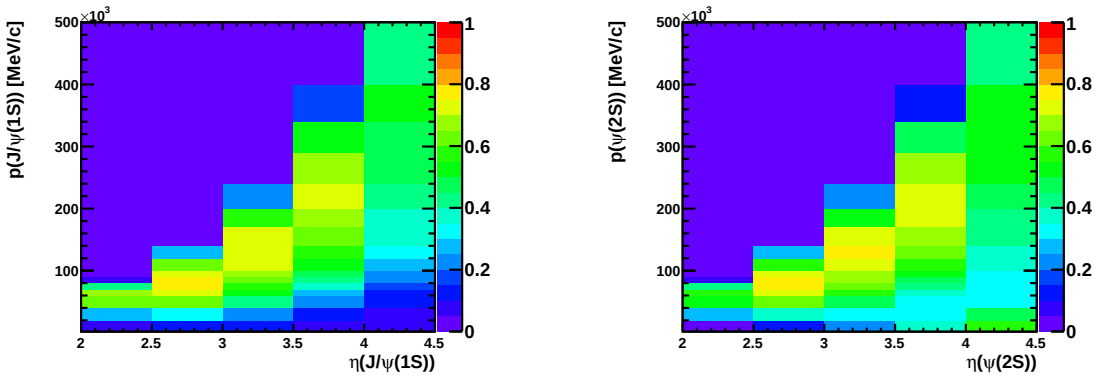

Figure 4.8: Selection efficiency for $J/\psi(1S)$ and $\psi(2S)$.

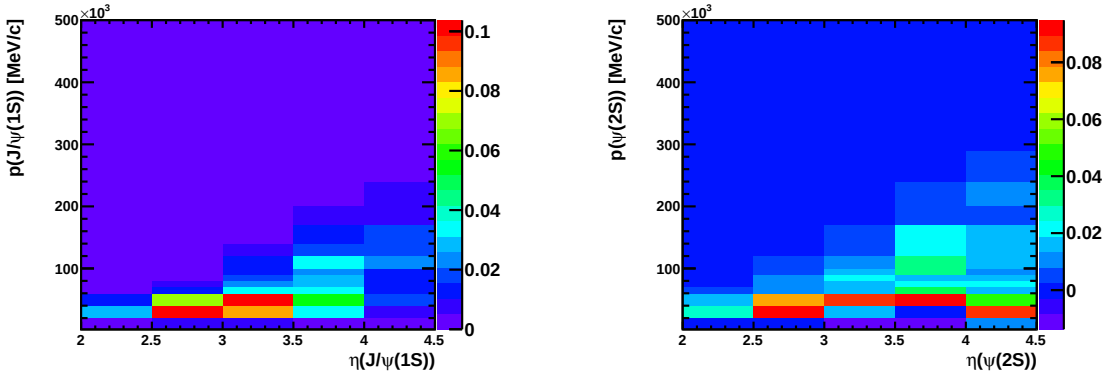

Figure 4.9: Normalized distribution of the data events for $J/\psi(1S)$ and $\psi(2S)$ in η and p.

$$\varepsilon_{\text{sel}}(2S) = 0.47 \pm 0.03 \tag{4.8}$$

and the ratio is:

$$\frac{\varepsilon_{\text{sel}}(1S)}{\varepsilon_{\text{sel}}(2S)} = 0.83 \pm 0.06 \tag{4.9}$$

The statistical uncertainty on the efficiency ratio will be assigned as a systematic uncertainty on the final result.

4.9 Reconstruction Efficiency

The same calculation as for the $\Upsilon(nS)$-states (Section 3.9) is used to determine the reconstruction efficiency of the $\psi(nS)$-states in bins of η and p. The results are shown in Fig. 4.10.

The calculated reconstruction efficiency for $J/\psi(1S)$ is:

$$\varepsilon_{\text{rec}}(1S) = 0.2544 \pm 0.0015 \tag{4.10}$$

for $\psi(2S)$ it is:

$$\varepsilon_{\text{rec}}(2S) = 0.300 \pm 0.023 \tag{4.11}$$

and the ratio is:

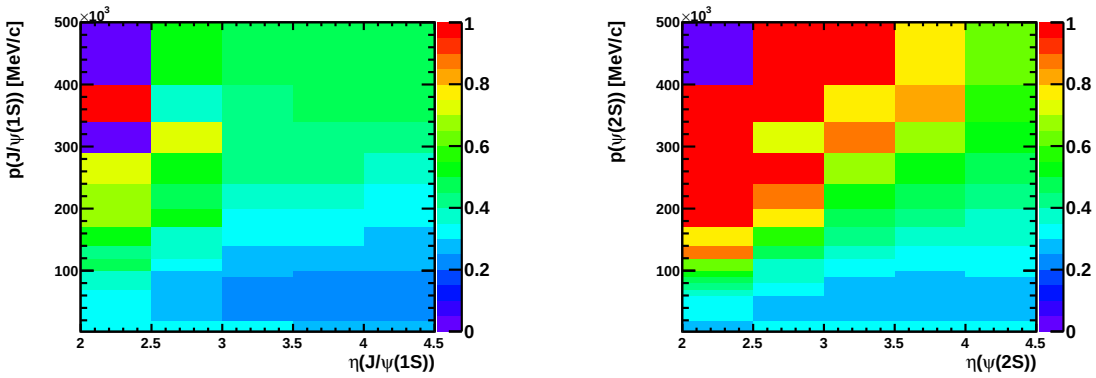

Figure 4.10: Reconstruction efficiencies for $\Upsilon(1S)$ and $\Upsilon(2S+3S)$.

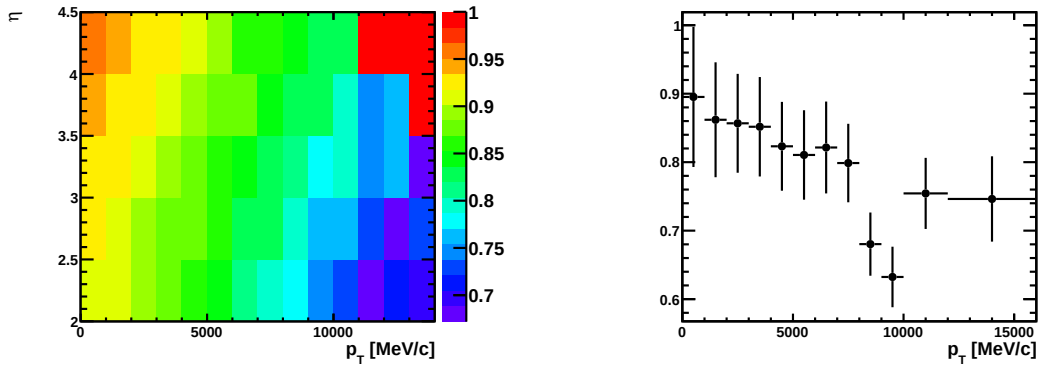

Figure 4.11: Fraction of prompt $J/\psi(1S)$ as a function of p_T and η [1] and $\psi(2S)$ as a function of p_T [2].

$$\frac{\varepsilon_{\text{rec}}(1S)}{\varepsilon_{\text{rec}}(2S)} = 0.85 \pm 0.07 \tag{4.12}$$

The statistical uncertainty on the efficiency ratio will be assigned as a systematic uncertainty on the final result.

4.10 Prompt Charmonia

We are only interested in prompt production of $\psi(nS)$, not in $\psi(nS)$ produced by decays like $X_b \to J/\psi(1S)X$ or $X_b \to \psi(2S)X$, where X_b is a b-hadron. We do not expect, to observe a suppression due to QGP effects in charmonium produced in decays of b-hadrons. Therefore we correct our result for the fraction of prompt charmonia. This fraction has been measured by LHCb as a function of the pseudo rapidity (η) and the transverse momentum (p_T) for $J/\psi(1S)$ [1] and for $\psi(2S)$ [2], it was found to depend only on p_T (Fig. 4.11).

To calculate the overall fraction of prompt charmonia, we weight each bin of these histograms (4.11) with the number of data-events it contains. For that we use sideband subtracted distributions of our data, for $J/\psi(1S)$ in η and p_T, for $\psi(2S)$ in p_T and normalize them (like in Section 4.8 and 4.9). Integration of the weighted histograms results in the fraction of prompt charmonia, which is for the ground state:

$$f_{\text{prompt}}(1S) = 0.883 \pm 0.006 \tag{4.13}$$

for $\psi(2S)$ it is:

$$f_{\text{prompt}}(2S) = 0.83 \pm 0.07 \tag{4.14}$$

and the ratio is:

$$\frac{f_{\text{prompt}}(2S)}{f_{\text{prompt}}(1S)} = 0.94 \pm 0.09 \tag{4.15}$$

The uncertainty on the ratio is obtained by simple error propagation assuming no correlation between $f_{\text{prompt}}(1S)$ and $f_{\text{prompt}}(2S)$. The ratio is compatible with 1 within the uncertainty.

4.11 Final Result

We combine all previous results, using Eq. (4.1) and obtain for the charmonium-suppression in the phase space of the $\psi(nS)$ of $2.0 \leq \eta \leq 4.5$, $2\,\text{GeV/c} \leq p \leq 500\,\text{GeV/c}$ and $p_T \leq 14\,\text{GeV/c}$:

$$\gamma = \frac{\psi(2S)}{J/\psi(1S)} = 0.184 \pm 0.013_{\text{stat}} \pm 0.024_{\text{sys}} \pm 0.019_{\mathcal{B}} \pm 0.017_{\text{prompt}} \tag{4.16}$$

The statistical uncertainty is due to the event yield. The uncertainties on the trigger, selection and reconstruction efficiency are added in quadrature to the systematic uncertainty. The third uncertainty is a consequence of the uncertainties on the branching fractions for $J/\psi(1S) \to \mu^+\mu^-$ and $\psi(2S) \to \mu^+\mu^-$ in Table 1.2 and the last uncertainty is due to the correction for prompt charmonia. We included in the calculation of the suppression factor $\psi(nS)$ mesons which have been decay products of other charmonium states, like in the decay $\chi_{c0} \to J/\psi(1S)\gamma$. We have not corrected for those decays.

5 Conclusion

We found the following value for the bottomonium suppression:

$$\gamma = \frac{\Upsilon(2S+3S)}{\Upsilon(1S)} = 0.489 \pm 0.004_{\text{stat}} \pm 0.021_{\text{sys}} \pm 0.034_{\mathcal{B}} \tag{5.1}$$

The $\Upsilon(nS)$ have pseudo rapidity between 2 and 4.5, the momenta are in the range of 2 GeV/c to 500 GeV/c. The muons of the $\Upsilon(nS)$ decay have transverse momenta bigger than 1.5 GeV/c and the pseudo rapidity is in the same range as for the $\Upsilon(nS)$. The dominating uncertainty is due to the branching fractions. Our result fits very well the theoretical predictions calculated by [6] and quoted in Table 1.4. But it is inconsistent with the value of 0.78 ± 0.18 measured by [9]. The reason for this may be the differenent center-of-mass energy. Another reason could be the the different phase spaces tested by the two measurements, but in first order no phase space dependence is expected [6] although the theory has no detailed predictions. It would be interesting to measure the suppression factor at other energies to compare with [9] and to test for a possible dependence on the energy.
The value for the prompt charmonium suppression is:

$$\gamma = \frac{\psi(2S)}{J/\psi(1S)} = 0.184 \pm 0.013_{\text{stat}} \pm 0.024_{\text{sys}} \pm 0.019_{\mathcal{B}} \pm 0.017_{\text{prompt}} \tag{5.2}$$

The $\psi(nS)$ are in the same phase space as the $\Upsilon(nS)$, but have in addition transverse momenta smaller than 14 GeV/c. The decay muons are in the same phase space as for the bottomonium. For both, bottomonium and charmonium, events from radiative decays of higher states are not corrected for.

Bibliography

[1] R. Aaij et al. [LHCb Collaboration]: *Measurement of the J/ψ production in pp collisions at $\sqrt{s} = 7$ TeV*, Eur. Phys. J. C 71 (2011) 1645, arXiv:1103.0423 [hep-ex]

[2] R. Aaij et al. [LHCb Collaboration]: *Measurement of $\psi(2S)$ meson production in pp collisions at $\sqrt{s} = 7$ TeV*, LHCb-PAPER-2011-045, arXiv:1204.1258 [hep-ex]

[3] R. Aaji et al. [LHCb collaboration]: *Measurement of $\sigma(pp \to b\bar{b}X)$ at $\sqrt{s} = 7$ TeV in the forward region*, Physics Letters B 694 209-216, 2010

[4] R. Aaji et al. [LHCb collaboration]: *Strong Constraints on the Rare Decays $B_s^0 \to \mu^+\mu^-$ and $B^0 \to \mu^+\mu^-$*, Phys. Rev. Lett. 108, 231801 (2012)

[5] J. Beringer et al. (Particle Data Group), Phys. Rev. D86, 010001 (2012)

[6] F. Brezinski, G. Wolschin: *Gluodissociation and screening of Υ states in PbPb collisions at $\sqrt{s_{NN}} = 2.76$ TeV*, Physics Letters B 707 (2012) 534-538

[7] E. Jans: *The LHCb detector*, Proceedings of the DPF-2009 Conference, Detroit, MI, July 27-31, 2009

[8] M. Pepe Altarelli: *LHCb: detector performance and first physics results*, arXiv:1105.5330v1 [hep-ex] 26 May 2011

[9] The CMS Collaboration: *Suppression of excited Υ states in PbPb collisions at $\sqrt{s_{NN}} = 2.76$ TeV*, arXiv:1105.4894v1 [nucl-ex] 24 May 2011

[10] The LHCb Collaboration: *The LHCb detector at the LHC*, 2008 JINST 3 S08005

[11] The LHCb Collaboration: *Measurement of J/ψ production cross-section at $\sqrt{s} = 7$ TeV*, LHCb-CONF-2010-010

[12] The LHCb Collaboration: *Measurement of $\psi(2S)$ production cross-section at $\sqrt{s} = 7$ TeV*, LHCb-CONF-2011-026

[13] C. Wong: Physical Review C 72, 034906, 2005